arXiv:2002.03704v4 [cs.LG] 10 Mar 2021

Liberty or Depth: Deep Bayesian Neural Nets Do Not Need Complex Weight Posterior Approximations

Sebastian Farquhar **Lewis Smith** **Yarin Gal**

OATML, Department of Computer Science
University of Oxford
sebastian.farquhar@cs.ox.ac.uk

Abstract

We challenge the longstanding assumption that the mean-field approximation for variational inference in Bayesian neural networks is severely restrictive, and show this is not the case in *deep* networks. We prove several results indicating that deep mean-field variational weight posteriors can induce similar distributions in function-space to those induced by shallower networks with complex weight posteriors. We validate our theoretical contributions empirically, both through examination of the weight posterior using Hamiltonian Monte Carlo in small models and by comparing diagonal- to structured-covariance in large settings. Since complex variational posteriors are often expensive and cumbersome to implement, our results suggest that using mean-field variational inference in a deeper model is both a practical and theoretically justified alternative to structured approximations.

1 Introduction

While performing variational inference (VI) in Bayesian neural networks (BNNs) researchers often make the 'mean-field' approximation which assumes that the posterior distribution factorizes over weights (i.e., diagonal weight covariance). Researchers have assumed that using this mean-field approximation in BNNs is a severe limitation. This has motivated extensive exploration of VI methods that explicitly model correlations between weights (see Related Work §2). Furthermore, Foong et al. [2020] have identified pathologies in single-hidden-layer mean-field regression models, and have conjectured that these might exist in deeper models as well.

However, the rejection of mean-field methods comes at a price. Structured covariance methods have worse time complexity (see Table 1) and even efficient implementations take over twice as long to train an epoch as comparable mean-field approaches [Osawa et al., 2019]. Moreover, recent work has succeeded in building mean-field BNNs which perform well (e.g., Wu et al. [2019]), creating a puzzle for those who have assumed that the mean-field approximation is too restrictive.

We argue that for larger, deeper, networks the mean-field approximation matters less to the downstream task of approximating posterior predictive distributions *over functions* than it does in smaller shallow networks. In essence: simple parametric functions need complicated weight-distributions to induce rich distributions in function-space; but complicated parametric functions can induce the same function-space distributions with simple weight-distributions. Complex covariance is computationally expensive and often cumbersome to implement though, while depth can be easy to implement and cheap to compute with standard deep learning packages.

Rather than introducing a new method, we provide empirical and theoretical evidence that some of the widely-held assumptions present in the research community about the strengths and weaknesses of existing methods are incorrect. Even when performing VI in weight-space, one does not care

34th Conference on Neural Information Processing Systems (NeurIPS 2020), Vancouver, Canada.

about the posterior distribution over the weights, $p(\boldsymbol{\theta}|\mathcal{D})$, for its own sake. Most decision processes and performance measures like accuracy or log-likelihood only depend on the induced posterior predictive, the distribution over function values $p(y|\mathbf{x}, \mathcal{D}) = \int p(y|\mathbf{x}, \boldsymbol{\theta})p(\boldsymbol{\theta}|\mathcal{D})d\boldsymbol{\theta}$. One way to have an expressive approximate posterior predictive is to have a simple likelihood function and a rich approximate posterior over the weights, $q(\boldsymbol{\theta})$, to fit to $p(\boldsymbol{\theta}|\mathcal{D})$. But another route to a rich approximate predictive posterior is to have a simple $q(\boldsymbol{\theta})$, and a rich likelihood function, $p(y|\mathbf{x}, \boldsymbol{\theta})$—e.g., a deeper model mapping $\mathbf{x}$ to y. These arguments lead us to examine two subtly different hypotheses: one comparing mean-field variational inference (MFVI) to VI with a full- or structured- covariance; and the other comparing the expressive power of a mean-field BNN directly to the true posterior predictive over function values, $p(y|\mathbf{x}, \mathcal{D})$:

Weight Distribution Hypothesis. For any BNN with a full-covariance weight distribution, there exists a deeper BNN with a mean-field weight distribution that induces a "similar" posterior predictive distribution in function-space.

True Posterior Hypothesis. For any sufficiently deep and wide BNN, and for any posterior predictive, there exists a *mean-field* distribution over the weights of that BNN which induces the same distribution over function values as that induced by the posterior predictive, with arbitrarily small error.

The Weight Distribution Hypothesis would suggest that we can trade a shallow complex-covariance BNN for deeper mean-field BNN without sacrificing the expressiveness of the induced function distribution. We start by analyzing linear models and then use these results to examine deep neural networks with piecewise linear activations (e.g., ReLUs). In linear deep networks—with no non-linear activations—a model with factorized distributions over the weights can be "collapsed" through matrix multiplication into a single *product matrix* with a complex induced distribution. In §3, we analytically derive the covariance between elements of this product matrix. We show that the induced product matrix distribution is very rich, and that three layers of weights suffice to allow non-zero correlations between any pair of product matrix elements. Although we do not show that any full-covariance weight distribution can be represented in this way, we do show that the Matrix Variate Gaussian distribution—a commonly used structured-covariance approximation—is a special case of a three-layer product matrix distribution, allowing MFVI to model rich covariances. In §4 we introduce the *local product matrix*—a novel analytical tool for bridging results from linear networks into deep neural networks with piecewise-linear activations like ReLUs. We apply this more general tool to prove a partial local extension of the results in §3.

The True Posterior Hypothesis states that mean-field weight distributions can approximate the true predictive posterior distribution, and moreover we provide evidence that VI can discover these distributions. In §5 we prove that the True Posterior Hypothesis is true for BNNs with at least two hidden layers, given arbitrarily wide models. In §6.1, we investigate the optima discovered by mean-field VI using Hamiltonian Monte Carlo [Neal, 1995]. We show empirically that even in smaller networks, as the model becomes deeper, we lose progressively less information by using a mean-field approximation rather than full-covariance. We also conduct experiments with deep convolutional architectures and find no significant difference in performance between a particular diagonal and full covariance method (SWAG, [Maddox et al., 2019]), an effect which we find is consistent with results from other papers working with various posterior approximations.

2 Related Work

The mean-field approximation has been widely used for variational inference (VI) [Hinton and van Camp, 1993, Graves, 2011, Blundell et al., 2015] (see Appendix A for a brief primer on VI methods for Bayesian neural networks). But researchers have assumed that using the mean-field approximation for Bayesian inference in neural networks is a severe limitation since MacKay [1992] wrote that for BNNs the "diagonal approximation is no good because of the strong posterior correlations in the parameters." Full-covariance VI was there-

	Complexity	
	Time	Parameter
MFVI [Hinton and van Camp, 1993]	K^2	K^2
Full [Barber and Bishop, 1998]	K^{12}	K^4
MVG [Louizos and Welling, 2016]	K^3	K^2
MVG-Inducing Point [ibid.]	$K^2 + P^3$	K^2
Noisy KFAC [Zhang et al., 2018]	K^3	K^2

Table 1: Complexity for forward pass in K—the number of hidden units for a square weight layer. Mean-field VI has better time complexity and avoids a numerically unstable matrix inversion. Inducing point approximations can help, but inducing dimension P is then a bottleneck.

fore introduced by Barber and Bishop [1998], but it requires many parameters and has poor time complexity. The intractability of full-covariance VI led to extensive research into structured-covariance approximations [Louizos and Welling, 2016, Zhang et al., 2018, Mishkin et al., 2019, Oh et al., 2019]. However, these still have unattractive time complexity compared with mean-field variational inference (MFVI) (see Table 1) and are not widely used. Researchers have also sought to model richer approximate posterior distributions [Jaakkola and Jordan, 1998, Mnih and Gregor, 2014, Rezende and Mohamed, 2015, Louizos and Welling, 2017] or to perform VI directly on the function—but this becomes intractable for high-dimensional input [Sun et al., 2019].

Despite widespread assertions that the mean-field approximation results in a problematically restricted approximate posterior in deep neural networks, there has been no work *in deep neural networks* demonstrating this; theoretical analysis and experimental work supporting this claim is typically based on shallow network architectures. For example, recent work has argued that the mean-field approximation is too restrictive and has identified pathologies in *single-layer* mean-field VI for regression [Foong et al., 2020]. We emphasise their theorems are entirely consistent with ours: we agree that the mean-field approximation could be problematic in small and single-layer models. While Foong et al. [2020] conjecture that the pathologies they identify extend to deeper models and classification problems, they do not prove this (see Appendix B).

In contrast, Hinton and van Camp [1993] hypothesized that even with a mean-field approximating distribution, during optimization the parameters will find a version of the network where this restriction is least costly, which our work bears out. Moreover, others have successfully applied mean-field approximate posteriors [Khan et al., 2018, Osawa et al., 2019, Wu et al., 2019, Farquhar et al., 2020] or even more restrictive approximations [Swiatkowski et al., 2020] in deep models, by identifying and correcting problems like gradient variance that have nothing to do with the restrictiveness of the mean-field approximation.

3 Emergence of Complex Covariance in Deep Linear Mean-Field Networks

In this section, we prove that a restricted version of the Weight Distribution Hypothesis is true in linear networks. Although we are most interested in neural networks that have non-linear activations, linear neural networks can be analytically useful [Saxe et al., 2014]. In §4 we give first steps to extend this analysis to non-linear activations.

Defining a Product Matrix: Setting the activation function of a neural network, $\phi(\cdot)$, to be the identity turns a neural network into a deep linear model. Without non-linearities the weights of the model just act by matrix multiplication. L weight matrices for a deep linear model can therefore be 'flattened' through matrix multiplication into a single weight matrix which we call the *product matrix*—$M^{(L)}$. For a BNN, the weight distributions induce a distribution over the elements of this product matrix. Because the model is linear, there is a one-to-one mapping between distributions induced over elements of this product matrix and the distribution over linear functions $y = M^{(L)}\mathbf{x}$. This offers us a way to examine exactly which sorts of distributions can be induced by a deep linear model on the elements of a product matrix, and therefore on the resulting function-space.

Covariance of the Product Matrix: We derive the analytic form of the covariance of the product matrix in Appendix D.1, explicitly finding the covariance of $M^{(2)}$ and $M^{(3)}$ as well as the update rule for increasing L. These results hold for *any* factorized weight distribution with finite first- and second-order moments, not just Gaussian weights. Using these expressions, we show:

Proposition 1. *For $L \geq 3$, the product matrix $M^{(L)}$ of factorized weight matrices can have non-zero covariance between any and all pairs of elements. That is, there exists a set of mean-field weight matrices $\{W^{(l)} | 1 \leq l < L\}$ such that $M^{(L)} = \prod W^{(l)}$ and the covariance between any possible pair of elements of the product matrix:*

$$\mathrm{Cov}(m_{ab}^{(L)}, m_{cd}^{(L)}) \neq 0, \tag{1}$$

where $m_{ij}^{(L)}$ are elements of the product matrix in the i^{th} row and j^{th} column, and for any possible indexes a, b, c, and d.

This shows that a deep mean-field linear model is able to induce function-space distributions which would require covariance between weights in a shallower model. This is weaker than the Weight

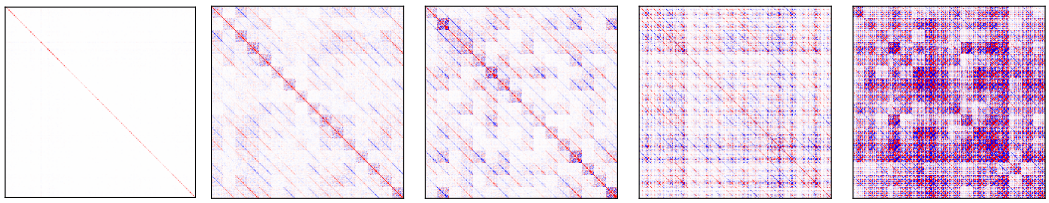

(a) One weight matrix.

(b) 5-layer product matrix. (Linear)

(c) 10-layer product matrix. (Linear)

(d) 5-layer local product matrix. (Leaky ReLU)

(e) 10-layer local product matrix. (Leaky ReLU)

Figure 1: Covariance heatmap for mean-field approximate posteriors trained on FashionMNIST. (a) A single layer has diagonal covariance. (b-c) In a deep linear model the *product matrix* composed of L mean-field weight matrices has off-diagonal covariance induced by the mean-field layers. Redder is more positive, bluer more negative. (d-e) For piecewise non-linear activations we introduce 'local product matrices' (defined in §4) with similar covariance. Shared activations introduce extra correlations. This lets us extend results from linear to piecewise-linear neural networks.

Distribution Hypothesis, because we do not show that all possible fully parameterized covariance matrices between elements of the product matrix can be induced in this way.[1] However, we emphasise that the expressible covariances become very complex. Below, we show that a lower bound on their expressiveness exceeds a commonly used structured-covariance approximate distribution.

Numerical Simulation: To build intuition, in Figure 1a–c we visualize the covariance between entries of the product matrix from a deep mean-field VI linear model trained on FashionMNIST. Even though each weight matrix makes the mean-field assumption, the product develops off-diagonal correlations. The experiment is described in more detail in Appendix C.1.

How Expressive is the Product Matrix? We show that the Matrix Variate Gaussian (MVG) distribution is a special case of the mean-field product matrix distribution. The MVG distribution is used as a structured-covariance approximation by e.g., Louizos and Welling [2016], Zhang et al. [2018] to approximate the covariance of weight matrices while performing variational inference.[2] We prove in Appendix D.2:

Proposition 2. *The Matrix Variate Gaussian (Kronecker-factored) distribution is a special case of the distribution over elements of the product matrix. In particular, for $M^{(3)} = ABC$, $M^{(3)}$ is distributed as an MVG random variable when A and C are deterministic and B has its elements distributed as fully factorized Gaussians with unit variance.*

This directly entails in the linear case that:

Weak Weight Distribution Hypothesis–MVG. For any deep linear model with an MVG weight distribution, there exists a deeper linear model with a mean-field weight distribution that induces the same posterior predictive distribution in function-space.

Remark 1. *This is a **lower bound** on the expressiveness of the product matrix. We have made* very *strong restrictions on the parameterization of the weights for the sake of an interpretable result. The unconstrained expressiveness of the product matrix covariance given in Appendix D.1 is much greater. Also note, we do not propose using this in practice, it is purely an analysis tool.*

[1] E.g., a full-covariance layer has more degrees of freedom than a three-layer mean-field product matrix (one of the weaknesses of full-covariance in practice). An L-layer product matrix of $K \times K$ Gaussian weight matrices has $2LK^2$ parameters, but one full-covariance weight matrix has K^2 mean parameters and $K^2(K^2+1)/2$ covariance parameters. Note also that the distributions over the elements of a product matrix composed of Gaussian layers are not in general Gaussian (see Appendix D.3 for more discussion of this point).

[2] In some settings, MVG distributions can be indicated by the Kronecker-factored or K-FAC approximation. In MVGs, the covariance between elements of an $n_0 \times n_1$ weight matrix can be described as $\Sigma = V \otimes U$ where U and V are positive definite real scale matrices of shape $n_0 \times n_0$ and $n_1 \times n_1$.

4 Weight Dist. Hypothesis in Deep Piecewise-Linear Mean-Field BNNs

Neural networks use non-linear activations to increase the flexibility of function approximation. On the face of it, these non-linearities make it impossible to consider product matrices. In this section we show how to define the *local product matrix*, which is an extension of the product matrix to widely used neural networks with piecewise-linear activation functions like ReLUs or Leaky ReLUs. For this we draw inspiration from a proof technique by Shamir et al. [2019] which we extend to stochastic matrices. This analytical tool can be used for any stochastic neural network with piecewise linear activations. Here, we use it to extend Lemma 1 to neural networks with piecewise-linear activations.

Defining a Local Product Matrix: Neural nets with piecewise-linear activations induce piecewise-linear functions. These piecewise-linear neural network functions define hyperplanes which partition the input domain into regions within which the function is linear. Each region can be identified by a sign vector that indicates which activations are 'switched on'. We show in Appendix D.4.1:

Lemma 1. *Consider an input point $\mathbf{x}^* \in \mathcal{D}$. Consider a realization of the model weights $\boldsymbol{\theta}$. Then, for any $\mathbf{x}^*$, the neural network function $f_{\boldsymbol{\theta}}$ is linear over some compact set $\mathcal{A}_{\boldsymbol{\theta}} \subset \mathcal{D}$ containing $\mathbf{x}^*$. Moreover, $\mathcal{A}_{\boldsymbol{\theta}}$ has non-zero measure for almost all $\mathbf{x}^*$ w.r.t. the Lebesgue measure.*

Using a set of N realizations of the weight parameters $\Theta = \{\boldsymbol{\theta}_i \text{ for } 1 \leq i \leq N\}$ we construct a product matrix within $\mathcal{A} = \bigcap_i \mathcal{A}_{\boldsymbol{\theta}_i}$. Since each $f_{\boldsymbol{\theta}_i}$ is linear over $\mathcal{A}$, the activation function can be replaced by a diagonal matrix which multiplies each row of its 'input' by a constant that depends on which activations are 'switched on' (e.g., 0 or 1 for a ReLU). This allows us to compute through matrix multiplication a product matrix of L weight layers $M^{(L)}_{\mathbf{x}^*,\boldsymbol{\theta}_i}$ corresponding to each function realization within $\mathcal{A}$. We construct a local product matrix random variate $P_{\mathbf{x}^*}$, for a given $\mathbf{x}^*$, within $\mathcal{A}$, by sampling these $M^{(L)}_{\mathbf{x}^*,\boldsymbol{\theta}_i}$. The random variate $P_{\mathbf{x}^*}$ is therefore such that y given $\mathbf{x}^*$ has the same distribution as $P_{\mathbf{x}^*}\mathbf{x}^*$ within $\mathcal{A}$. This distribution can be found empirically at a given input point, and resembles the product matrices from linear settings (see Figure 1d–e).

Covariance of the Local Product Matrix: We can examine this local product matrix in order to investigate the covariance between its elements. We prove in D.4 that:

Proposition 3. *Given a mean-field distribution over the weights of neural network f with piecewise linear activations, f can be written in terms of the local product matrix $P_{\mathbf{x}^*}$ within $\mathcal{A}$.*

For $L \geq 3$, for activation functions which are non-zero everywhere, there exists a set of weight matrices $\{W^{(l)} | 1 \leq l < L\}$ such that all elements of the local product matrix have non-zero off-diagonal covariance:

$$\text{Cov}(p^{\mathbf{x}^*}_{ab}, p^{\mathbf{x}^*}_{cd}) \neq 0, \tag{2}$$

where $p^{\mathbf{x}^*}_{ij}$ is the element at the i^{th} row and j^{th} column of $P_{\mathbf{x}^*}$.

Proposition 3 is weaker than the Weight Distribution Hypothesis. Once more, we do not show that all full-covariance weight distributions can be exactly replicated by a deeper factorized network. We now have non-linear networks which give richer functions, potentially allowing richer covariance, but the non-linearities have introduced analytical complications. However, it illustrates the way in which deep factorized networks can emulate rich covariance in a shallower network.

Remark 2. *Proposition 3 is restricted to activations that are non-zero everywhere although we believe that in practice it will hold for activations that can be zero, like ReLU. If the activation can be zero then, for some $\mathbf{x}^*$, enough activations could be 'switched off' such that the effective depth is less than three. This seems unlikely in a trained network, since it amounts to throwing away most of the network's capacity, but we cannot rule it out theoretically. In Appendix D.4 we empirically corroborate that activations are rarely all 'switched off' in multiple entire layers.*

Numerical Simulation: We confirm empirically that the local product matrix develops complex off-diagonal correlations using a neural networkwith Leaky ReLU activations trained on FashionMNIST using mean-field variational inference. We estimate the covariance matrix using 10,000 samples of a trained model (Figure 1d–e). Just like in the linear case (Figure 1a–c), as the model gets deeper the induced distribution on the product matrix shows complex off-diagonal covariance. There are additional correlations between elements of the product matrix based on which activation pattern is predominantly present at that point in input-space. See Appendix C.1 for further experimental details.

5 True Posterior Hypothesis in Two-Hidden-Layer Mean-Field Networks

We prove the True Posterior Hypothesis using the universal approximation theorem (UAT) due to Leshno et al. [1993] in a stochastic adaptation by Foong et al. [2020]. This shows that a BNN with a mean-field approximate posterior with at least two layers of hidden units can induce a function-space distribution that matches any true posterior distribution over function values arbitrarily closely, given arbitrary width. Our proof formalizes and extends a remark by Gal [2016, p23] concerning multi-modal posterior predictive distributions.

Proposition 4. *Let $p(\mathbf{y} = \mathbf{Y}|\mathbf{x}, \mathcal{D})$ be the probability density function for the posterior predictive distribution of any given multivariate regression function, with $\mathbf{x} \in \mathbb{R}^D$, $\mathbf{y} \in \mathbb{R}^K$, and $\mathbf{Y}$ the posterior predictive random variable. Let $f(\cdot)$ be a Bayesian neural network with two hidden layers. Let $\hat{\mathbf{Y}}$ be the random vector defined by $f(\mathbf{x})$. Then, for any $\epsilon, \delta > 0$, there exists a set of parameters defining the neural network f such that the absolute value of the difference in probability densities for any point is bounded:*

$$\forall \mathbf{y}, \mathbf{x}, i: \quad \Pr\left(|p(y_i = \hat{Y}_i) - p(y_i = Y_i|\mathbf{x}, \mathcal{D})| > \epsilon\right) < \delta, \tag{3}$$

so long as: the activations of f are non-polynomial, non-periodic, and have only zero-measure non-monotonic regions, the first hidden layer has at least $D + 1$ units, the second hidden layer has an arbitrarily large number of units, the cumulative density function of the posterior predictive is continuous in output-space, and the probability density function is continous and finite non-zero everywhere. Here, the probability bound is with respect to the distribution over a subset of the weights described in the proof, $\boldsymbol{\theta}_{\text{Pr}}$, while one weight distribution $\boldsymbol{\theta}_Z$ remains to induce the random variable $\hat{\mathbf{Y}}$.

The full proof is provided in Appendix D.5. Intuitively, we define a $q(\boldsymbol{\theta})$ to induce an arbitrary distribution over hidden units in the first layer and using the remaining weights and hidden layer we approximate the inverse cumulative density function of the true posterior predictive by the UAT. It follows from Proposition 4 that it is possible, in principle, to learn a mean-field approximate posterior which induces the true posterior distribution over predictive functions. Our proof strengthens a result by Foong et al. [2020] which considers only the first two moments of the posterior predictive.

There are important limitations to this argument to bear in mind. First, the UAT might require arbitrarily wide models. Second, to achieve arbitrarily small error δ it is necessary to reduce the weight variance. Both of these might result in very low weight-space evidence lower-bounds (ELBOs). Third it may be difficult in practice to choose a prior in weight-space that induces the desired prior in function space. Fourth, although the distribution in weight space that maximizes the marginal likelihood will also maximize the marginal likelihood in function-space within that model class, the same is not true of the weight-space ELBO and functional ELBO. Our proposition therefore does not show that such an approximate posterior will be found by VI. We investigate this empirically below.

6 Empirical Validation

We have already considered the Weight Distribution Hypothesis theoretically and confirmed through numerical simulation that deeper factorized networks can show off-diagonal covariance in the product matrix. We now examine the True Posterior Hypothesis empirically from two directions. First, we examine the true posterior of the weight distribution using Hamiltonian Monte Carlo and consider the extent to which the mean-field assumption makes it harder to match a mode of the true posterior. Second, we work off the assumption that a worse approximation of the true posterior would result in significantly worse performance on downstream tasks, and we show that we are unable to find such a difference in both large- and small-scale settings.

6.1 Examining the True Posterior with Hamiltonian Monte Carlo

Proposition 4 proves the True Posterior Hypothesis in sufficiently wide models of two or more layers. Here, we examine the true posterior distribution using Hamiltonian Monte Carlo (HMC) and show that even in narrow deep models there are modes of the true posterior that are approximately mean-field. We examine a truly full-covariance posterior, not even assuming that layers are independent of each other, unlike Barber and Bishop [1998] and most structured covariance approximations.

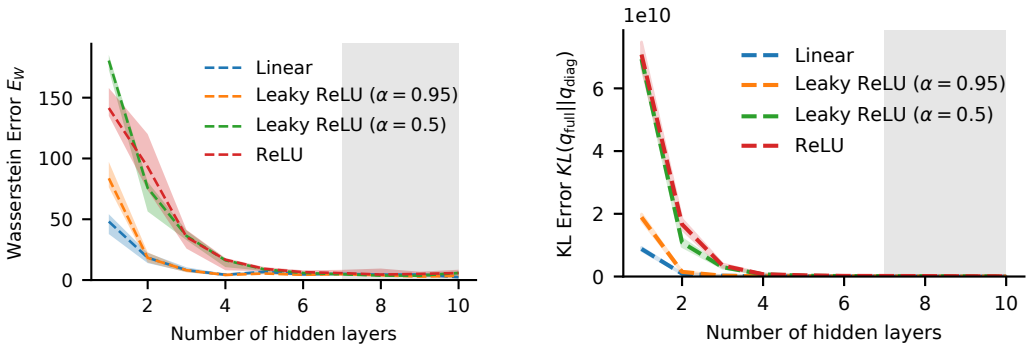

(a) Wasserstein Error.

(b) KL-divergence Error.

Figure 2: For all activations and both error measures, large error in shallow networks almost disappears with depth. All models have ∼1,000 parameters. Shaded depths: less reliable HMC samples.

Methodology: To approximate the true posterior distribution—$p(\boldsymbol{\theta})$—we use the No-U-turn HMC sampling method [Hoffman and Gelman, 2014]. We then aim to determine how much worse a mean-field approximation to these samples is than a full-covariance one. To do this, we fit a full-covariance Gaussian distribution to the samples from the true posterior—$\hat{q}_{\text{full}}(\boldsymbol{\theta})$—and a Gaussian constrained to be fully-factorized—$\hat{q}_{\text{diag}}(\boldsymbol{\theta})$. We deliberately do not aim to sample from multiple modes of the true posterior—VI is an essentially mode-seeking method.[3] Each point on the graph represents an average over 20 restarts (over 2.5 million model evaluations per point on the plot). For all depths, we adjust the width so that the model has roughly 1,000 parameters and train on the binary classification 'two-moons' task. We report the sample test accuracies and acceptance rates in Appendix C.3 and provide a full description of the method. We consider two measures of distance:

1. **Wasserstein Distance:** We estimate the L_2-Wasserstein distance between samples from the true posterior and each Gaussian approximation. Define the Wasserstein Error:
$$E_W = W(p(\boldsymbol{\theta}), \hat{q}_{\text{diag}}(\boldsymbol{\theta})) - W(p(\boldsymbol{\theta}), \hat{q}_{\text{full}}(\boldsymbol{\theta})). \tag{4}$$
If the true posterior is fully factorized, then $E_W = 0$. The more harmful a fully-factorized assumption is to the approximate posterior, the larger E_W will be.
2. **KL-divergence:** We estimate the KL-divergence between the two Gaussian approximations. Define the KL Error:
$$E_{KL} = KL\big(\hat{q}_{\text{full}}(\boldsymbol{\theta}) \parallel \hat{q}_{\text{diag}}(\boldsymbol{\theta})\big). \tag{5}$$
This represents a worst-case information loss from using the diagonal Gaussian approximation rather than a full-covariance Gaussian, measured in nats (strictly, the infimum information loss under any possible discretization [Gray, 2011]). $E_{KL} = 0$ when the mode is naturally diagonal, and is larger the worse the approximation is. (Note that we do not directly involve $p(\boldsymbol{\theta})$ here because KL-divergence does not follow the triangle inequality.)

Note that we are only trying to establish how costly the *mean-field* approximation is relative to full covariance, not how costly the *Gaussian* approximation is.

Results: In Figure 2a we find that the Wasserstein Error introduced by the mean-field approximation is large in shallow networks but falls rapidly as the models become deeper. In Figure 2b we similarly show that the KL-divergence Error is large for shallow networks but rapidly decreases. Although these models are small, this is very direct evidence that there are mean-field modes of the true posterior of a deeper Bayesian neural network.

In all cases, this is true regardless of the activation we consider, or whether we use any activation at all. Indeed we find that a non-linear model with a very shallow non-linearity (LeakyReLU with $\alpha = 0.95$) behaves very much like a deep linear model, while one with a sharper but still shallow non-linearity ($\alpha = 0.5$) behaves much like a ReLU. This suggests that the shape of the true posterior modes varies

[3] In fact, in order to ensure that we do not accidentally capture multiple modes, we use the dominant mode of a mixture of Gaussians model selected using the Bayesian Information Criterion (see Appendix C.3 for details).

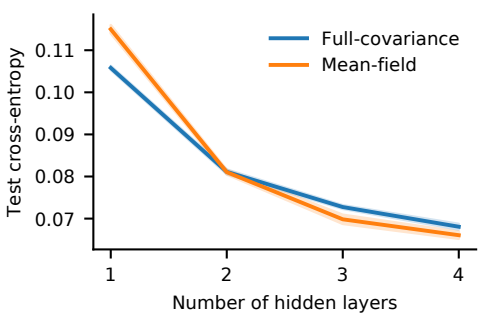

Figure 3: Full- vs diagonal-covariance. After two hidden layers mean-field matches full-covariance. Iris dataset.

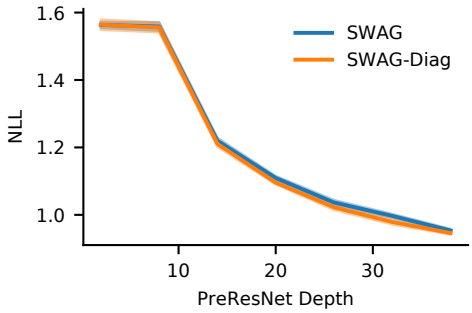

Figure 4: CIFAR-100. Diagonal- and Structured-SWAG show similar log-likelihood in PresNets of varying depth.

between linear models and non-linear ones more as a matter of degree than kind, suggesting that our analysis in §3 has bearing on the non-linear case.

6.2 Factorization and Downstream Task Performance

Here, we compare the performance of Bayesian neural networks with complex posterior approximations to those with mean-field approximations. We show that over a spectrum of model sizes, performance does not seem to be greatly determined by the approximation.

Depth in Full- and Diagonal-covariance Variational Inference. Training with full-covariance variational inference is intractable, except for very small models, because of optimization difficulties. In Figure 3, we show the test cross-entropy of small models of varying depths on the Iris dataset from the UCI repository. With one layer of hidden units the full-covariance posterior achieves lower cross-entropy. For deeper models, however, the mean field network matches the full-covariance one. Full details of the experiment can be found in Appendix C.2.

Structured- and Diagonal-covariance Uncertainty on CIFAR-100. Although we cannot compute samples from the true posterior in larger models, we attempt an approximate investigation using SWAG [Maddox et al., 2019]. This involves fitting a Gaussian distribution to approximate Stochastic Gradient-Markov Chain Monte Carlo samples on CIFAR-100. SWAG approximates the Gaussian distribution with a low rank empirical covariance matrix, while SWAG-Diag uses a full-factorized Gaussian. The resulting distributions are some indication of large-model posterior behaviour, but cannot carry too much weight. We show in Figure 4 that there is no observable difference in negative log-likelihood between the diagonal and low-rank approximation (or accuracy, see Appendix C.4). All of the models considered have more than two layers of hidden units (the minimum size of a PresNet). This suggests that there is a mode of the true posterior over weights for these deeper models that is sufficiently mean-field that a structured approximation provides little or no benefit. It also suggests that past a threshold of two hidden layers, further depth is not essential.

Large-model Mean-field Approximations on Imagenet. The performance of mean-field and structured-covariance methods on large-scale tasks can give some sense of how restrictive the mean-field approximation is. Mean-field methods have been shown to perform comparably to structured methods in large scale settings like Imagenet, both in accuracy and measures of uncertainty like log-likelihood and expected calibration error (ECE) (see Table 2). For VOGN [Osawa et al., 2019] which explicitly optimizes for a mean-field variational posterior, the mean-field model is marginally better in all three measures. For SWAG, the accuracy is marginally better and log-likelihood and ECE marginally worse for the diagonal approximation. This is consistent with the idea that there are some modes of large models that are approximately mean-field (which VOGN searches for but SWAG does not) but that not all modes are. These findings offer some evidence that the importance of structured covariance is at least greatly diminished in large-scale models, and may not be worth the additional computational expense and modelling complexity. A table with standard deviations and comparison for CIFAR-10 is provided in Appendix C.5.

Architecture	Method	Covariance	Accuracy	NLL	ECE
ResNet-18	VOGN[‡]	Diagonal	67.4%	1.37	0.029
ResNet-18	Noisy K-FAC[††]	MVG	66.4%	1.44	0.080
DenseNet-161	SWAG-Diag[†]	Diagonal	78.6%	0.86	0.046
DenseNet-161	SWAG[†]	Low-rank	78.6%	0.83	0.020
ResNet-152	SWAG-Diag[†]	Diagonal	80.0%	0.86	0.057
ResNet-152	SWAG[†]	Low-rank	79.1%	0.82	0.028

Table 2: Imagenet diagonal- and structure-covariance methods. Both approximations have similar accuracies, log-likelihoods, and expected calibration errors. Suggests that covariance matters less in large models, as predicted. [†] [Maddox et al., 2019]. [‡] [Osawa et al., 2019]. [††] [Zhang et al., 2018] as reported by Osawa et al. [2019].

7 Discussion

We have argued that deeper models with mean-field approximate posteriors can act like shallower models with much richer approximate posteriors. In deep linear models, a product matrix with rich covariance structure is induced by mean-field approximate posterior distributions—in fact, the Matrix Variate Gaussian is a special case of this induced distribution for at least three weight layers (two layers of hidden units) (§3). We provided a new analytical tool to extend results from linear models to piecewise linear neural networks (e.g., ReLU activations): the local product matrix. In addition, examination of the induced covariance in the local product matrix (§4) and posterior samples with HMC (§6.1) suggest that the linear results are informative about non-linear networks.

Moreover, we have proved that neural networks with at least two layers of hidden units and mean-field weight distributions can approximate any posterior distribution over predictive functions. In sufficiently deep models, the performance gap between mean-field and structured-covariance approximate posteriors becomes small or non-existent, suggesting that modes of the true posterior in large settings may be approximately mean-field.

Our work challenges the previously unchallenged assumption that mean-field VI fails because the posterior approximation is too restrictive. Instead, rich posterior approximations and deep architectures are complementary ways to create rich approximate posterior distributions over predictive functions. So long as a network has at least two layers of hidden units, increasing the parameterization of the neural network allows some modes of the true posterior over weights to become approximately mean-field. This means that approximating posterior functions becomes easier for mean-field variational inference in larger models—making it more important to address other challenges for MFVI at scale.

Acknowledgements

We would especially like to thank Adam Cobb for his help applying the Hamiltorch package [Cobb et al., 2019]; Angelos Filos for his help with the experiment in Figure 5; and Andrew Foong, David Burt, and Yingzhen Li for their conversations regarding the proof of Proposition 4. The authors would further like to thank for their comments and conversations Wendelin Boehmer, David Burt, Adam Cobb, Gregory Farquhar, Andrew Foong, Raza Habib, Andreas Kirsch, Yingzhen Li, Clare Lyle, Michael Hutchinson, Sebastian Ober, Hippolyt Ritter, and Jan Wasilewski as well as anonymous reviewers who have generously contributed their time and expertise.

This work was supported by the EPSCRC CDTs for Cyber Security and for Autonomous Intelligent Machines and Systems at the University of Oxford. It was also supported by the Alan Turing Institute.

Broader Impact

Our work addresses a growing need for scalable neural network systems that are able to express sensible uncertainty. Sensible uncertainty is essential in systems that make important decisions in production settings. Despite that, the most performant production systems often rely on large deterministic deep learning models. Historically, uncertainty methods have often prioritized smaller

settings where more theoretically rigorous methods could be applied. Our work demonstrates the theoretical applicability of cheap uncertainty approximation methods that do not attempt to model complex correlations between weight distributions in those large-scale settings. This resolves something the field has assumed is a tension between good uncertainty and powerful models—we show that some modes of the variational weight posterior might be closer to mean-field in bigger models. So using a bigger model causes more restrictive approximation methods to become more accurate.

In principle, this could allow Bayesian neural networks with robust uncertainty to be deployed in a wide range of settings. If we are right, this would be a very good thing. The main downside risk of our research is that if we are wrong, and people deploy these systems and incorrectly rely on their uncertainty measures, then this could result in accidents caused by overconfidence. We therefore recommend being extremely cautious in how a business or administrative decision process depends on any uncertainty measures in critical settings, as is already good practice for non-uncertainty-aware decisions and in non-neural network uncertain machine learning systems.

References

David Barber and Christopher M Bishop. Ensemble Learning in Bayesian Neural Networks. In *Neural Networks and Machine Learning*, pages 215–237. Springer, 1998. 2, 6.1, A

Charles Blundell, Julien Cornebise, Koray Kavukcuoglu, and Daan Wierstra. Weight Uncertainty in Neural Networks. *Proceedings of the 32nd International Conference on Machine Learning*, 37: 1613–1622, 2015. 2, A

Lennart Bondesson. A Class of Probability Distributions that is Closed with Respect to Addition as Well as Multiplication of Independent Random Variables. *Journal of Theoretical Probability*, 28 (3):1063–1081, September 2015. D.3

Adam D. Cobb, Atılım Güneş Baydin, Andrew Markham, and Stephen J. Roberts. Introducing an Explicit Symplectic Integration Scheme for Riemannian Manifold Hamiltonian Monte Carlo. *arXiv*, October 2019. 7, C.3

Sebastian Farquhar, Michael Osborne, and Yarin Gal. Radial Bayesian Neural Networks: Robust Variational Inference In Big Models. *Proceedings of the 23rd International Conference on Artificial Intelligence and Statistics*, 2020. 2

Andrew Y. K. Foong, David R. Burt, Yingzhen Li, and Richard E. Turner. On the Expressiveness of Approximate Inference in Bayesian Neural Networks. *arXiv*, February 2020. 1, 2, 5, 5, B, 2, B, D.5.2, D.5

Yarin Gal. Uncertainty in Deep Learning. *PhD Thesis*, 2016. 5, D.5

Micah Goldblum, Jonas Geiping, Avi Schwarzschild, Michael Moeller, and Tom Goldstein. Truth or backpropaganda? An empirical investigation of deep learning theory. In *International Conference on Learning Representations*, September 2019. 4

Alex Graves. Practical Variational Inference for Neural Networks. *Neural Information Processing Systems*, 2011. 2

Robert M. Gray. *Entropy and Information Theory*. Springer US, second edition, 2011. ISBN 978-1-4419-7969-8. doi: 10.1007/978-1-4419-7970-4. 2

Kaiming He, Xiangyu Zhang, Shaoqing Ren, and Jian Sun. Deep Residual Learning for Image Recognition. *CVPR*, 7(3):171–180, 2016.

Geoffrey Hinton and Drew van Camp. Keeping Neural Networks Simple by Minimizing the Description Length of the Weights. *Proceedings of the 6th Annual ACM Conference on Computational Learning Theory*, 1993. 2

Matthew D Hoffman and Andrew Gelman. The No-U-Turn Sampler: Adaptively Setting Path Lengths in Hamiltonian Monte Carlo. *Journal of Machine Learning Research*, 15:1593–1623, 2014. 6.1, C.3

Tommi S. Jaakkola and Michael I. Jordan. Improving the Mean Field Approximation Via the Use of Mixture Distributions. In Michael I. Jordan, editor, *Learning in Graphical Models*, NATO ASI Series, pages 163–173. Springer Netherlands, Dordrecht, 1998. doi: 10.1007/978-94-011-5014-9_6. 2

Mohammad Emtiyaz Khan, Didrik Nielsen, Voot Tangkaratt, Wu Lin, Yarin Gal, and Akash Srivastava. Fast and Scalable Bayesian Deep Learning by Weight-Perturbation in Adam. *International Conference on Machine Learning*, 2018. 2

Moshe Leshno, Vladimir Ya. Lin, Allan Pinkus, and Shimon Schocken. Multilayer feedforward networks with a nonpolynomial activation function can approximate any function. *Neural Networks*, 6(6):861–867, January 1993. ISSN 08936080. doi: 10.1016/S0893-6080(05)80131-5. 5, D.5.1, D.5.2

Christos Louizos and Max Welling. Structured and Efficient Variational Deep Learning with Matrix Gaussian Posteriors. *International Conference on Machine Learning*, pages 1708–1716, 2016. 2, 3

Christos Louizos and Max Welling. Multiplicative Normalizing Flows for Variational Bayesian Neural Networks. In *International Conference on Machine Learning*, pages 2218–2227, July 2017. 2

David J. C. MacKay. A Practical Bayesian Framework for Backpropagation Networks. *Neural Computation*, 4(3):448–472, 1992. 2, A

Wesley Maddox, Timur Garipov, Pavel Izmailov, Dmitry Vetrov, and Andrew Gordon Wilson. A Simple Baseline for Bayesian Uncertainty in Deep Learning. *Neural Information Processing Systems*, December 2019. 1, 6.2, 2, C.4

Aaron Mishkin, Frederik Kunstner, Didrik Nielsen, Mark Schmidt, and Mohammad Emtiyaz Khan. SLANG: Fast Structured Covariance Approximations for Bayesian Deep Learning with Natural Gradient. *arXiv:1811.04504 [cs, stat]*, January 2019. 2

Andriy Mnih and Karol Gregor. Neural Variational Inference and Learning in Belief Networks. *International Conference on Machine Learning*, June 2014. 2

Guido Montúfar, Razvan Pascanu, Kyunghyun Cho, and Yoshua Bengio. On the Number of Linear Regions of Deep Neural Networks. *Neural Information Processing Systems*, June 2014. D.4.1

Radford M. Neal. *Bayesian Learning for Neural Networks*. PhD Thesis, University of Toronto, 1995. 1

Changyong Oh, Kamil Adamczewski, and Mijung Park. Radial and Directional Posteriors for Bayesian Neural Networks. *Bayesian Deep Learning Workshop at NeurIPS*, February 2019. 2

Kazuki Osawa, Siddharth Swaroop, Anirudh Jain, Runa Eschenhagen, Richard E. Turner, Rio Yokota, and Mohammad Emtiyaz Khan. Practical Deep Learning with Bayesian Principles. *arXiv:1906.02506 [cs, stat]*, June 2019. 1, 2, 6.2, 2, C.5

Sashank J. Reddi, Satyen Kale, and Sanjiv Kumar. On the Convergence of Adam and Beyond. *International Conference on Learning Representations*, February 2018.

Danilo Jimenez Rezende and Shakir Mohamed. Variational Inference with Normalizing Flows. *International Conference on Machine Learning*, 2015. 2

Walter Rudin. *Principles of Mathematical Analysis*. McGraw Hill, 3rd edition, 1976. D.5.1, D.5

A. M. Saxe, J. L. McClelland, and S Ganguli. Exact solutions to the nonlinear dynamics of learning in deep linear neural networks. *International Conference on Learning Representations*, 2014. 3

Adi Shamir, Itay Safran, Eyal Ronen, and Orr Dunkelman. A Simple Explanation for the Existence of Adversarial Examples with Small Hamming Distance. *arXiv*, January 2019. 4

M. D. Springer and W. E. Thompson. The Distribution of Products of Beta, Gamma and Gaussian Random Variables. *SIAM Journal on Applied Mathematics*, 18(4):721–737, 1970. ISSN 0036-1399. D.3

Shengyang Sun, Guodong Zhang, Jiaxin Shi, and Roger Grosse. Functional variational Bayesian Neural Networks. *International Conference on Learning Representations*, 2019. 2, A

Jakub Swiatkowski, Kevin Roth, Bastiaan S. Veeling, Linh Tran, Joshua V. Dillon, Jasper Snoek, Stephan Mandt, Tim Salimans, Rodolphe Jenatton, and Sebastian Nowozin. The k-tied Normal Distribution: A Compact Parameterization of Gaussian Mean Field Posteriors in Bayesian Neural Networks. *International Conference on Machine Learning*, 2020. 2

Yeming Wen, Paul Vicol, Jimmy Ba, Dustin Tran, and Roger Grosse. Flipout: Efficient Pseudo-Independent Weight Perturbations on Mini-Batches. *International Conference on Learning Representations*, April 2018.

Anqi Wu, Sebastian Nowozin, Edward Meeds, Richard E Turner, Jose Miguel Hernandez-Lobato, and Alexander L Gaunt. Deterministic Variational Inference for Robust Bayesian Neural Networks. *International Conference on Learning Representations*, 2019. 1, 2

Han Xiao, Kashif Rasul, and Roland Vollgraf. Fashion-MNIST: A Novel Image Dataset for Benchmarking Machine Learning Algorithms. *arXiv*, August 2017.

Guodong Zhang, Shengyang Sun, David Duvenaud, and Roger Grosse. Noisy Natural Gradient as Variational Inference. *International Conference on Machine Learning*, 2018. 2, 3, 2, C.5

A Introduction to Variational Inference in Bayesian Neural Networks

A Bayesian neural network (BNN) places a distribution over the weights of a neural network [MacKay, 1992]. We hope to infer the posterior distribution over the weights given the data, $p(\boldsymbol{\theta}|\mathcal{D})$—although ultimately we are interested in a posterior distribution over functions, as described by Sun et al. [2019]. Because this is intractable, we seek an approximate posterior $q(\boldsymbol{\theta})$ to be as close as possible to the posterior over the weights. Variational inference (VI) is one method for estimating that approximate posterior, in which we pick an approximating distribution and minimize the KL-divergence between it and the true posterior. This KL divergence is the Evidence Lower Bound (ELBO), expressed using the prior over the weight distributions $p(\boldsymbol{\theta})$. We therefore minimize the negative ELBO:

$$\mathcal{L}_{MFVI} = \overbrace{KL\big(q(\boldsymbol{\theta}) \parallel p(\boldsymbol{\theta})\big)}^{\text{prior regularization}} - \overbrace{\mathbb{E}\left[\log p(y|\mathbf{x}, \boldsymbol{\theta})\right]}^{\text{data likelihood}}. \tag{6}$$

For the full-covariance Gaussian approximate posterior [Barber and Bishop, 1998], the model weights for each layer $\boldsymbol{\theta}_i$ are distributed according to the multivariate Gaussian distribution $\mathcal{N}(\boldsymbol{\mu}_i, \Sigma_i)$. This is already a slight approximation, as it assumes layers are independent of each other. This is important for our analysis in §3 and §4, though note that the experiment in §6.1 does not assume any independence between layers.

The mean-field approximation restricts Σ_i to be a diagonal covariance matrix, or equivalently assumes that the probability distribution can be expressed as a product of individual weight distributions:

$$\mathcal{N}(\boldsymbol{\mu}_i, \Sigma_i) = \prod_j \mathcal{N}(\mu_{ij}, \sigma_{ij}). \tag{7}$$

The mean-field approximation greatly reduces the computational cost of both forward and backwards propagation, and reduces the number of parameters required to store the model from order n^2 in the number of weights to order n. The implementation of mean-field variational inference which we use is based on Blundell et al. [2015], who show how to use a stochastic estimator of the ELBO.

B Discussions of Foong et al. 2020

Our work discusses some similar topics to those discussed by Foong et al. [2020], in work which was developed in parallel to this paper. In particular, they reach a different conclusion as to the value of mean-field variational inference in *deep* BNNs. We find their work insightful, but we think it is important to be very precise about where their results do and do not apply, in order to best understand their implications. Here, we briefly describe several of their main results, emphasising that our analysis is not in conflict with any of their proofs.

Empirically, they focus on the posterior distribution over function outputs in small models, where they find that the learned function distributions with mean-field variational inference for regression tend to be overconfident, even in slightly deeper models. We also find that in relatively small regression tasks MFVI does not perform particularly well, which aligns with their results. However, below, we note that in fact their theoretical results suggest that MFVI may have problems with regression that do not extend to classification tasks. Moreover, it is important to note that the largest of their experiments considers data with only 16-dimensional inputs, with only 55 training points and very small models with 4 layers of 50 hidden units. In contrast, our work analyses much larger models and datasets, where it is admittedly harder to compare to a reference posterior in function-space. However, these are the situations where MFVI would be more typical for deep learning. We therefore feel that, while there is significant room for further investigation, on the balance of the current evidence MFVI seems quite appropriate for large-scale deep learning especially in classification tasks.

Foong et al. [2020] base much of their interpretation on the inability of single-layer mean-field networks to have appropriate 'in-between' uncertainty. That is, they observe that if a model is trained on data in two regions of input space which are separated, it ought to be able to be significantly more uncertain between those two regions. They prove their Theorem 1 which states that the variance of the function expressed by a single-layer mean-field network between two points cannot be greater than the sum of the variances of the function at those points, subject to a number of very important caveats. Our work is largely concerned with models with more than a single hidden layer, where

their theorem does not apply. Nevertheless, Foong et al. [2020] hypothesize the pathologies that they identify might extend to deeper settings, so we note some further limitations of their proof.

1. Theorem 1 applies to single- or multi-output regression models, and to the individual logits in classification models, but makes no predictions about the variance of classification *decisions* (because this depends on the variance of the argmax of the logits).
2. Theorem 1 is strongest in a 1-dimensional input space. In higher dimensions, Foong et al. [2020] show as a corollary that the 'in-between' variance is bounded by the sum of the variances of the hypercube of points including that space. But the number of such points grows exponentially with the dimensionality, meaning that in even only 10 dimensions, the in-between variance could be as much as 1024 times greater than the average edge variance. This means that in high-dimensional input spaces, this bound can be extremely loose and does not neccesarily preclude even single layer models from having significant 'in between' uncertainty.
3. The line-segments where Theorem 1 applies are not fully general. They must either go through the origin, or be orthogonal to one of the input basis vectors and cross a projection of the origin. This makes their result sensitive to translation and rotation of the input space. However, the authors do provide some empirical evidence that 'in between' uncertainty is too low on more general lines in input space for small models.

They also prove their Theorem 3, which establishes that deeper mean-field networks do not have the pathologies that apply in the limited single-layer regression settings identified in Theorem 1. We consider a similar result (Proposition 4) which is more general because it considers more than the first two moments of the distribution. Unlike Foong et al. [2020] we see this result as potentially promising that deep mean-field networks can be very expressive. This is perhaps because their empirical results suggest that deeper mean-field networks have poor performance in practice. This may be because their experiments mostly focus on low-dimensional data with small numbers of datapoints and comparatively small networks, while we consider the larger settings.

We note also that we find that deeper networks are able to show in-between uncertainty in regression, if not necessarily capture it as fully as something like HMC. In Figure 5 we show how increasing depth increases the ability of MFVI neural networks to capture in-between uncertainty even on low-dimensional data.

Here, each layer has 100 hidden units trained using mean-field variational inference on a sythetic dataset in order to demonstrate the possibility of 'in-between' uncertainty. Full experimental settings are provided in Table 3. The toy function used is $y = \sin(4(x - 4.3)) + \epsilon$ where $\epsilon \sim \mathcal{N}(0, 0.05^2)$. We sample 750 points in the interval $-2 \leq x \leq -1.4$ and another 750 points in the interval $1.0 \leq x \leq 1.8$. We considered a range of temperatures between 0.1 and 100 in order to select the right balance between prior and data. Note of course that while our figure in the main body suffices to demonstrate the existence claim that there are deep networks that perform well, of course a single case of a one-layer network performing badly does not show that all one-layer networks perform badly.

C Experimental Details

C.1 Full Description of Covariance Visualization

Here we provide details on the method used to produce Figure 1. The linear version of the visualization is discussed in §3 and the piecewise-linear version is discussed in §4.

In all cases, we train a neural network using mean-field variational inference in order to visualize the covariance of the product matrix. The details of training are provided in Table 4. The product matrix is calculated from the weight matrices of an L-layer network. In the linear case, this is just the matrix product of the L layers. In the piecewise-linear case the definition of the product matrix is described in more detail in Appendix D.4.2. All covariances are calculated using 10,000 samples from the converged approximate posterior. Note that for L weight matrtices there are $L - 1$ layers of hidden units.

We compare these learned product matrices, in Figure 6, to a randomly sampled product matrix. To do so, we sample weight layers whose entries are distributed normally. Each weight is sampled with

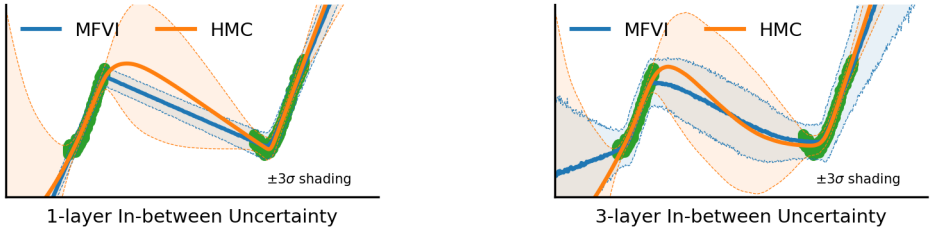

(a) 1-layer BNN

(b) 3-layer BNN

Figure 5: In-between uncertainty. With a single hidden layer, mean-field variational inference cannot capture in-between uncertainty at all in low-dimensional settings. But by adding more layers, we increase the ability to capture in-between uncertainty, though still not to the point of HMC. Note, of course, that neural networks are at their most useful with higher dimensional data where in-between uncertainty results are exponentially weaker.

Hyperparameter	Setting description
Architecture	MLP
Number of hidden layers	3
Layer Width	100
Activation	Leaky ReLU
Approximate Inference Algorithm	Mean-field VI (Flipout [Wen et al., 2018])
Optimization algorithm	Amsgrad [Reddi et al., 2018]
Learning rate	10^{-3}
Batch size	250
Variational training samples	1
Variational test samples	1
Temperature	65
Noise scale	0.05
Epochs	6000
Variational Posterior Initialization	Tensorflow Probability default
Prior	$\mathcal{N}(0, 1.0^2)$
Dataset	Toy (see text)
Number of training runs	1
Number of evaluation runs	1
Measures of central tendency	n.a.
Runtime per result	< 5m
Computing Infrastructure	Nvidia GTX 1060

Table 3: Experimental Setting—Toy Regression Visualization. Note that for these visualizations we are purely demonstrating the possibility of in-between uncertainty. As a result, a single training/evaluation run suffices to make an existence claim, so we do not do multiple runs in order to calculate a measure of central tendency.

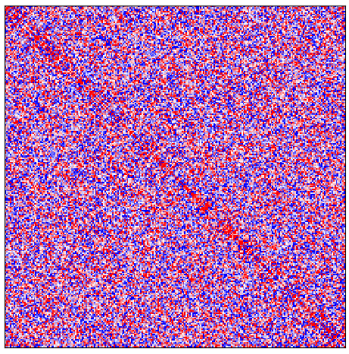

Figure 6: Unlike the covariance matrices of product matrix entries in models trained on real data, a randomly sampled product matrix does not show obvious block structure, though the noise makes it hard to be sure. This model has 5 linear layers.

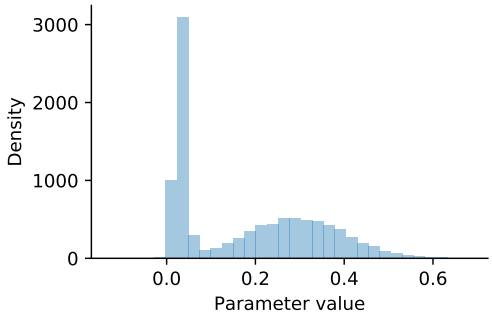

Figure 7: The local product matrix also allows the unimodal Gaussian layers to approximate multimodal distributions over product matrix entries. Here, we show an example density over a product matrix element, from a three-layer Leaky ReLU model with mean-field Gaussian distributions over each weight trained on FashionMNIST.

Hyperparameter	Setting description
Architecture	MLP
Number of hidden layers	0-9
Layer Width	16
Activation	Linear or Leaky Relu with $\alpha = 0.1$
Approximate Inference Algorithm	Mean-field Variational Inference
Optimization algorithm	Amsgrad [Reddi et al., 2018]
Learning rate	10^{-3}
Batch size	64
Variational training samples	16
Variational test samples	16
Epochs	10
Variational Posterior Initial Mean	He et al. [2016]
Variational Posterior Initial Standard Deviation	$\log[1 + e^{-3}]$
Prior	$\mathcal{N}(0, 0.23^2)$
Dataset	FashionMNIST [Xiao et al., 2017]
Preprocessing	Data normalized $\mu = 0$, $\sigma = 1$
Validation Split	90% train - 10% validation
Number of training runs	1
Number of evaluation runs	1
Measures of central tendency	n.a.
Runtime per result	$<$ 3m
Computing Infrastructure	Nvidia GTX 1080

Table 4: Experimental Setting—Covariance Visualization. Note that for these visualizations we are purely demonstrating the possibility of off-diagonal covariance. As a result, a single training/evaluation run suffices to make an existence claim, so we do not do multiple runs in order to calculate a measure of central tendency.

Hyperparameter	Setting description
Architecture	MLP
Number of hidden layers	1-4
Layer Width	4
Activation	Leaky Relu
Approximate Inference Algorithm	Variational Inference
Optimization algorithm	Amsgrad [Reddi et al., 2018]
Learning rate	10^{-3}
Batch size	16
Variational training samples	1
Variational test samples	1
Epochs	1000 (early stopping patience=30)
Variational Posterior Initial Mean	He et al. [2016]
Variational Posterior Initial Standard Deviation	$\log[1 + e^{-6}]$
Prior	$\mathcal{N}(0, 1.0^2)$
Dataset	Iris [Xiao et al., 2017]
Preprocessing	None.
Validation Split	100 train - 50 test
Number of training runs	100
Number of evaluation runs	100
Measures of central tendency	(See text.)
Runtime per result	< 5m
Computing Infrastructure	Nvidia GTX 1080

Table 5: Experimental Setting—Full Covariance.

standard deviation 0.3 and with a mean 0.01 and each weight matrix is 16x16. This visualization is with a linear product matrix of 5 layers.

Further, since researchers often critique a Gaussian approximate posterior because it is unimodal, we confirm empirically that multiple mean-field layers can induce a multi-modal product matrix distribution. In Figure 7 we show a density over an element of the local product matrix from three layers of weights in a Leaky ReLU BNN with $\alpha = 0.1$. The induced distribution is multi-modal. We visually examined the distributions over 20 randomly chosen entries of this product matrix and found that 12 were multi-modal. We found that without the non-linear activation, none of the product matrix entry distributions examined were multimodal, suggesting that the non-linearities in fact play an important role in inducing rich predictive distributions by creating modes corresponding to activated sign patterns.

C.2 Effect of Depth Measured on Iris Experimental Settings

We describe the full- and diagonal-covariance experiment settings in Table 5. We use a very small model on a small dataset because full-covariance variational inference is unstable, requiring a matrix inversion of a K^4 matrix for hidden unit width K. Unfortunately, for deeper models the initializations still resulted in failed training for some seeds. To avoid this issue, we selected the 10 best seeds out of 100 training runs, and report the mean and standard error for these. Because we treat full- and diagonal-covariance in the same way, the resulting graph is a fair reflection of their relative best-case merits, but not intended as anything resembling a 'real-world' performance benchmark.

Readers may consider the Iris dataset to be unhelpfully small, however this was a necessary choice. We note that the small number of training points creates a broad posterior, which is the best-case scenario for a full-covariance approximate posterior.

C.3 HMC Experimental Settings

We begin by sampling from the true posterior using HMC.

# Hidden Layers	ReLU		Leaky ReLU 0.5		Leaky ReLU 0.95		Linear	
	Test Acc.	Acceptance	Test Acc.	Acceptance	Test Acc.	Acceptance	Test Acc.	Acceptance
1	99.1%	84.8%	98.4%	84.9%	91.9%	85.4%	83.9%	78.0%
2	99.7%	77.0%	99.5%	73.9%	96.4%	76.3%	84.2%	44.4%
3	99.1%	58.0%	99.6%	46.3%	97.2%	74.5%	84.4%	37.0%
4	99.5%	62.2%	99.6%	50.9%	95.8%	68.2%	84.4%	43.2%
5	98.1%	61.8%	99.5%	53.8%	98.4%	62.4%	84.3%	35.2%
6	95.4%	78.5%	99.6%	51.0%	98.0%	62.6%	84.1%	33.7%
7	92.7%	68.1%	99.7%	54.6%	97.5%	59.7%	84.0%	33.0%
8	87.8%	68.3%	99.6%	49.7%	98.0%	62.5%	83.8%	36.4%
9	80.6%	73.9%	99.6%	46.3%	97.4%	60.2%	83.9%	36.5%
10	74.6%	74.9%	99.5%	45.7%	97.1%	61.8%	83.8%	40.4%

Table 6: HMC samples for ReLU networks are most accurate for smaller numbers of layers, the samples from deeper models may therefore be slightly less reliable. Acceptance rates tend to be with 10-20 percentage points of 65%, regarded as a good balance of exploration to avoiding unnecessary resampling. The more linear models are less accurate, as one would expect for a dataset that is not linearly separable.

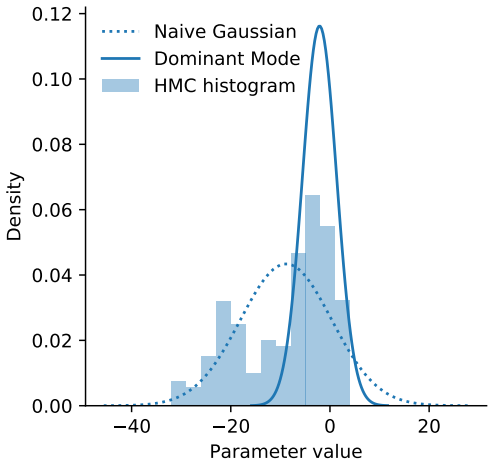

Figure 8: Example density for randomly chosen parameter from a ReLU network with three hidden layers. The HMC histogram is multimodal. If we picked the naive Gaussian fit, we would lie between the modes. By using a mixture model, we select the dominant mode, for which the Gaussian is a better fit.

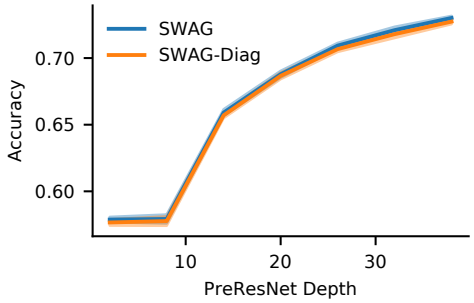

Figure 9: CIFAR-100. Accuracy for diagonal and low-rank covariance SWAG. Like log-likelihood, there is no clear difference in performance between these models, all of which are above the depth threshold implied by our work.

We use the simple two-dimensional binary classification 'make moons' task.[4] We use 500 training points (generated using $\text{random_state} = 0$). Using Cobb et al. [2019], we apply the No-U-turn Sampling scheme [Hoffman and Gelman, 2014] with an initial step size of 0.01. We use a burn-in phase with 10,000 steps targetting a rejection rate of 0.8. We then sample until we collect 1,000 samples from the true posterior, taking 100 leapfrog steps in between every sample used in order to ensure samples are less correlated. For each result, we recalculate the HMC samples 20 times with a different random seed. All chains are initialized at the optimum of a mean-field variational inference model in order to help HMC rapidly find a mode of the true posterior. We use a prior precision, normalizing constant, and τ of 1.0. The model is designed to have as close to 1000 non-bias parameters each time as possible, adjusting the width given the depth of the model. We observe that the accuracies for the ReLU network fall for the deeper models, suggesting that after about 7 layers the posterior estimate may become slightly less reliable (see Table 6). Acceptance rates are broadly in a sensible region for most of the chains.

[4] `https://scikit-learn.org/stable/modules/generated/sklearn.datasets.make_moons.html#sklearn.datasets.make_moons`

Using these samples, we find a Gaussian fit. For each model we fit a Gaussian mixture model with between 1 and 4 components and pick the one with the best Bayesian information criterion (see Figure 8). We then find the best diagonal fit to this distribution, which is a Gaussian distribution with the same mean and with a precision matrix equal to the inverse of the diagonal precision of the full-covariance Gaussian. We do this because variational inference uses the mode-seeking KL-divergence, so we are interested in the properties of a single Gaussian mode. The overall empirical covariance would lead to a mode-covering distribution, while optimizing the mode-seeking KL to the empirical distribution would of course result in a point-sized distribution centred at one of the HMC samples. Using one mode of a mixture of Gaussians is therefore the closest we can come to finding a single mode of the true posterior of the sort that VI might uncover. Note that we are therefore only considering one of the many modes of the true posterior—this is inevitable given the fact that there is a many-to-one correspondence between weight-distributions and function-distributions for neural networks.

Finally, we calculate the KL divergence between these two distributions. The graph reports the mean and shading reflects the standard error of the mean, though note that because all runs are initialized from the same point, this underestimates the overall standard error. All experiments in this an other sections were run on a desktop workstation with an Nvida 1080 GPU.

For the Wasserstein divergence, we estimate the distance between the empirical distributions formed by the HMC samples and samples from the full- and diagonal-covariance posterior approximation. We used the Python Optimal Transport package to estimate the divergence.

C.4 Diagonal- and Structured-SWAG at Varying Depths

We use the implementation of SWAG avaliable publicly at `https://github.com/wjmaddox/swa_gaussian`. We adapt their code to vary the depth of the PreResNet architecture for the values $2, 8, 14, 20, 26, 32, 38$. We use the hyperparameter settings used by the Maddox et al. [2019] for PreResNet154 on CIFAR100 on all datasets to train the models. We use 10 seeds to generate the error bars, which are plotted with one standard deviation. We use the same SWAG run to fit both the full and diagonal approximations, and use 30 samples in the forward pass.

C.5 Large Scale Experiments Descriptions

In Table 7 we show a complete version of Table 2 including the standard deviations over three runs (except for the Noisy K-FAC result where standard deviation was not provided). The standard deviations, of course, underestimate the true variability of the method in question on Imagenet as they only consider difference in random seed with the training configuration otherwise identical. Fuller descriptions of the experimental settings used by the authors are provided in the cited papers.

For CIFAR-10, we show similar results in Table 8. Here, authors compare a wider range of architectures, which show substantial variation in resulting accuracy. However, within the same architecture, there is little evidence of systematic differences between mean-field and structured-covariance methods and any differences which do appear are marginal. Note that Zhang et al. [2018] report difficulty applying batch normalization to mean-field methods, but Osawa et al. [2019] report no difficulties applying batch normalization for their mean-field variant of Noisy Adam. For this reason, we report the version of Noisy KFAC run without batch normalization to make it comparable with the results shown for Bayes-by-Backprop (BBB) and Noisy Adam. With batch normalization, Noisy KFAC gains some accuracy, reaching 92.0%, but this seems to be because of the additional regularization, not a property of the approximate posterior family.

D Proofs

D.1 Full Derivation of the Product Matrix Covariance

Proposition 1. *For $L \geq 3$, the product matrix $M^{(L)}$ of factorized weight matrices can have non-zero covariance between any and all pairs of elements. That is, there exists a set of mean-field weight matrices $\{W^{(l)} | 1 \leq l < L\}$ such that $M^{(L)} = \prod W^{(l)}$ and the covariance between any possible pair of elements of the product matrix:*

$$\text{Cov}(m_{ab}^{(L)}, m_{cd}^{(L)}) \neq 0, \tag{1}$$

Architecture	Method	Covariance	Accuracy	NLL	ECE
ResNet-18	VOGN‡	Diagonal	67.4% ± 0.263	1.37 ± 0.010	0.029 ± 0.001
ResNet-18	Noisy K-FAC††	MVG	66.4% ± n.d.	1.44 ± n.d.	0.080 ± n.d.
DenseNet-161	SWAG-Diag†	Diagonal	78.6% ± 0.000	0.86 ± 0.000	0.046 ± 0.000
DenseNet-161	SWAG†	Low-rank + Diag	78.6% ± 0.000	0.83 ± 0.000	0.020 ± 0.000
ResNet-152	SWAG-Diag†	Diagonal	80.0% ± 0.000	0.86 ± 0.000	0.057 ± 0.000
ResNet-152	SWAG†	Low-rank + Diag	79.1% ± 0.000	0.82 ± 0.000	0.028 ± 0.000

Table 7: Imagenet. Comparison of diagonal-covariance/mean-field (in grey) and structured-covariance methods on Imagenet. The differences on a given architecture between comparable methods is slight. † [Maddox et al., 2019]. ‡ [Osawa et al., 2019]. †† [Zhang et al., 2018] as reported by Osawa et al. [2019].

Architecture	Method	Covariance	Accuracy	NLL	ECE
VGG-16	SWAG-Diag†	Diagonal	93.7% ± 0.15	0.220 ± 0.008	0.027 ± 0.003
VGG-16	SWAG†	Low-rank + Diag	93.6% ± 0.10	0.202 ± 0.003	0.016 ± 0.003
VGG-16	Noisy Adam‡‡	Diagonal	88.2% ± n.d.	n.d.	n.d.
VGG-16	BBB‡‡	Diagonal	88.3% ± n.d.	n.d.	n.d.
VGG-16	Noisy KFAC‡‡	MVG	89.4% ± n.d.	n.d.	n.d.
PreResNet-164	SWAG-Diag†	Diagonal	96.0% ± 0.10	0.125 ± 0.003	0.008 ± 0.001
PreResNet-164	SWAG†	Low-rank + Diag	96.0% ± 0.02	0.123 ± 0.002	0.005 ± 0.000
WideResNet28x10	SWAG-Diag†	Diagonal	96.4% ± 0.08	0.108 ± 0.001	0.005 ± 0.001
WideResNet28x10	SWAG†	Low-rank + Diag	96.3% ± 0.08	0.112 ± 0.001	0.009 ± 0.001
ResNet-18	VOGN‡	Diagonal	84.3% ± 0.20	0.477 ± 0.006	0.040 ± 0.002
AlexNet	VOGN‡	Diagonal	75.5% ± 0.48	0.703 ± 0.006	0.016 ± 0.001

Table 8: CIFAR-10. For a given architecture, it does not seem that mean-field (grey) methods systematically perform worse than methods with structured covariance, although there is some difference in the results reported by different authors. † [Maddox et al., 2019]. ‡ [Osawa et al., 2019]. ‡‡ [Zhang et al., 2018].

where $m_{ij}^{(L)}$ are elements of the product matrix in the i^{th} row and j^{th} column, and for any possible indexes a, b, c, and d.

Proof. We begin by explicitly deriving the covariance between elements of the product matrix.

Consider the product matrix, $M^{(L)}$, which is the matrix product of an arbitrary weight matrix, $W^{(L)}$, with a mean field distribution over it's entries, and the product matrix with one fewer layers, $M^{(L-1)}$. Expressed in terms of the elements of each matrix in row-column notation this matrix multiplication can be written:

$$m_{ab}^{(L)} = \sum_{i=1}^{K_{L-1}} w_{ai}^{(L)} m_{ib}^{(L-1)}. \tag{8}$$

We make no assumption about K_{L-1} except that it is non-zero and hence the weights can be any rectangular matrix.[5] The weight matrix $W^{(L)}$ is assumed to have a mean-field distribution (the covariance matrix is zero for all off diagonal elements) with arbitrary means:

$$\begin{aligned} \mathrm{Cov}\big(w_{ac}^{(L)}, w_{bd}^{(L)}\big) = \Sigma_{abcd}^{(L)} = \delta_{ac}\delta_{bd}\sigma_{ab}^{(L)}; \\ \mathbb{E}\, w^{(L)}{}_{ab} = \mu_{ab}^{(L)}. \end{aligned} \tag{9}$$

δ are the Kronecker delta. Note that the weight matrix is 2-dimensional, but the covariance matrix is defined between every element of the weight matrix. While it can be helpful to regard it as 2-dimensional also, we index it with the four indices that define a pair of elements of the weight matrix.

[5] We set aside bias parameters, as they complicate the algebra, but adding them only strengthens the result because each bias term affects an entire row.

We begin by deriving the expression for the covariance of the L-layer product matrix $\mathrm{Cov}(m_{ab}^{(L)}, m_{cd}^{(L)})$. Using the definition of the product matrix in equation (8):

$$\mathrm{Cov}\big(m_{ab}^{(L)}, m_{cd}^{(L)}\big) = \mathrm{Cov}\big(\sum_i w_{ai}^{(L)} m_{ib}^{(L-1)}, \sum_j w_{cj}^{(L)} m_{jd}^{(L-1)}\big). \tag{10}$$

We then simplify this using the linearity of covariance (for brevity call the covariance of the product matrix $\hat{\Sigma}_{abcd}^{(L)}$):

$$\hat{\Sigma}_{abcd}^{(L)} = \sum_{ij} \mathrm{Cov}\big(w_{ai}^{(L)} m_{ib}^{(L-1)}, w_{cj}^{(L)} m_{jd}^{(L-1)}\big), \tag{11}$$

rewriting using the definition of covariance in terms of a difference of expectations:

$$= \sum_{ij} \mathbb{E}\left[w_{ai}^{(L)} m_{ib}^{(L-1)} w_{cj}^{(L)} m_{jd}^{(L-1)}\right] - \mathbb{E}\left[w_{ai}^{(L)} m_{ib}^{(L-1)}\right] \mathbb{E}\left[w_{cj}^{(L)} m_{jd}^{(L-1)}\right], \tag{12}$$

using the fact that by assumption the new layer is independent of the previous product matrix:

$$= \sum_{ij} \mathbb{E}\left[w_{ai}^{(L)} w_{cj}^{(L)}\right] \mathbb{E}\left[m_{ib}^{(L-1)} m_{jd}^{(L-1)}\right] - \mathbb{E}\left[w_{ai}^{(L)}\right] \mathbb{E}\left[w_{cj}^{(L)}\right] \mathbb{E}\left[m_{ib}^{(L-1)}\right] \mathbb{E}\left[m_{jd}^{(L-1)}\right], \tag{13}$$

and rewriting to expose the dependence on the covariance of $M^{(L-1)}$:

$$\begin{aligned}
= \sum_{ij} & \Big(\mathbb{E}\left[w_{ai}^{(L)} w_{cj}^{(L)}\right] - \mathbb{E}\left[w_{ai}^{(L)}\right] \mathbb{E}\left[w_{cj}^{(L)}\right]\Big) \\
& \cdot \Big(\mathbb{E}\left[m_{ib}^{(L-1)} m_{jd}^{(L-1)}\right] - \mathbb{E}\left[m_{ib}^{(L-1)}\right] \mathbb{E}\left[m_{jd}^{(L-1)}\right]\Big) \\
& + \mathbb{E}\left[w_{ai}^{(L)}\right] \mathbb{E}\left[w_{cj}^{(L)}\right] \Big(\mathbb{E}\left[m_{ib}^{(L-1)} m_{jd}^{(L-1)}\right] - \mathbb{E}\left[m_{ib}^{(L-1)}\right] \mathbb{E}\left[m_{jd}^{(L-1)}\right]\Big) \\
& + \mathbb{E}\left[m_{ib}^{(L-1)}\right] \mathbb{E}\left[m_{jd}^{(L-1)}\right] \Big(\mathbb{E}\left[w_{ai}^{(L)} w_{cj}^{(L)}\right] - \mathbb{E}\left[w_{ai}^{(L)}\right] \mathbb{E}\left[w_{cj}^{(L)}\right]\Big),
\end{aligned} \tag{14}$$

substituting the covariance:

$$\begin{aligned}
= \sum_{ij} & \mathrm{Cov}\Big(w_{ai}^{(L)}, w_{cj}^{(L)}\Big) \cdot \mathrm{Cov}\Big(m_{ib}^{(L-1)}, m_{jd}^{(L-1)}\Big) \\
& + \mathbb{E}\left[w_{ai}^{(L)}\right] \mathbb{E}\left[w_{cj}^{(L)}\right] \mathrm{Cov}\Big(m_{ib}^{(L-1)}, m_{jd}^{(L-1)}\Big) \\
& + \mathbb{E}\left[m_{ib}^{(L-1)}\right] \mathbb{E}\left[m_{jd}^{(L-1)}\right] \mathrm{Cov}\Big(w_{ai}^{(L)}, w_{cj}^{(L)}\Big).
\end{aligned} \tag{15}$$

This gives us a recursive expression for the covariance of the product matrix.

It is straightforward to substitute in our expressions for mean and variance in a mean-field network provided in equation (9), where we use the fact that the initial $M^{(1)}$ product matrix is just a single mean-field layer.

In this way, we show that:

$$\begin{aligned}
\hat{\Sigma}_{abcd}^{(2)} &= \sum_{ij} \Big(\delta_{ac}\delta_{ij}\sigma_{ai}^{(2)}\Big) \cdot \Big(\delta_{ij}\delta_{bd}\sigma_{ib}^{(1)}\Big) \\
&\qquad + \mu_{ai}^{(2)} \mu_{cj}^{(2)} \Big(\delta_{ij}\delta_{bd}\sigma_{ib}^{(1)}\Big) + \mathbb{E}\left[m_{ib}^{(1)}\right] \mathbb{E}\left[m_{jd}^{(1)}\right] \Big(\delta_{ac}\delta_{ij}\sigma_{ai}^{(2)}\Big) \qquad (16) \\
&= \sum_i \delta_{ac}\delta_{bd}\sigma_{ai}^{(2)}\sigma_{ib}^{(1)} + \delta_{bd}\mu_{ai}^{(2)}\mu_{ci}^{(2)}\sigma_{ib}^{(1)} + \delta_{ac}\mu_{ib}^{(1)}\mu_{id}^{(1)}\sigma_{ai}^{(2)}. \qquad (17)
\end{aligned}$$

The first term of equation (17) has the Kronecker deltas $\delta_{ac}\delta_{bd}$ meaning that it contains diagonal entries in the covariance matrix. The second term has only δ_{bd} meaning it contains entries for the covariance between weights that share a column. The third term has only δ_{ac} meaning it contains entries for the covariance between weights that share a row.

This covariance of the product matrix already has some off-diagonal terms, but it does not yet contain non-zero covariance for weights that share neither a row nor a column.

But we can repeat the process and find $\hat{\Sigma}^{(3)}_{abcd}$ using equation (15) and our expression for $\hat{\Sigma}^{(2)}_{ibjd}$:

$$\hat{\Sigma}^{(3)}_{abcd} = \sum_{ij}\left(\delta_{ac}\delta_{ij}\sigma^{(3)}_{ai}\right)\cdot\hat{\Sigma}^{(2)}_{ibjd} + \mu^{(3)}_{ai}\mu^{(3)}_{cj}\hat{\Sigma}^{(2)}_{ibjd} + \mathbb{E}\left[m^{(2)}_{ib}\right]\mathbb{E}\left[m^{(2)}_{jd}\right]\left(\delta_{ac}\delta_{ij}\sigma^{(3)}_{ai}\right) \tag{18}$$

$$\begin{aligned}
&= \sum_{ij}\left(\delta_{ac}\delta_{ij}\sigma^{(3)}_{ai}\right)\cdot\sum_{k}\left(\delta_{ij}\delta_{bd}\sigma^{(2)}_{ik}\sigma^{(1)}_{kb} + \delta_{bd}\mu^{(2)}_{ik}\mu^{(2)}_{jk}\sigma^{(1)}_{kb} + \delta_{ij}\mu^{(1)}_{kb}\mu^{(1)}_{kd}\sigma^{(2)}_{ik}\right)\\
&\quad + \mu^{(3)}_{ai}\mu^{(3)}_{cj}\cdot\sum_{k}\left(\delta_{ij}\delta_{bd}\sigma^{(2)}_{ik}\sigma^{(1)}_{kb} + \delta_{bd}\mu^{(2)}_{ik}\mu^{(2)}_{jk}\sigma^{(1)}_{kb} + \delta_{ij}\mu^{(1)}_{kb}\mu^{(1)}_{kd}\sigma^{(2)}_{ik}\right)\\
&\quad + \mu^{(2)}_{ib}\mu^{(2)}_{jd}\left(\delta_{ac}\delta_{ij}\sigma^{(3)}_{ai}\right).
\end{aligned} \tag{19}$$

It is the term in red which has no factors of Kronecker deltas in any of the indices a, b, c, or d. It is therefore present in all elements of the covariance matrix of the product matrix, regardless of whether they share one or both index. This shows that, so long as the distributional parameters themselves are non-zero, the product matrix can have a fully non-zero covariance matrix for $L = 3$.

We note that there are many weight matrices for which the resulting covariance is non-zero everywhere—we think this is actually typical. Indeed, empirically, we found that for any network we cared to construct, we were unable to find covariances that *were* zero anywhere. However, for our existance proof, we simply note that for any matrix in which all the means are positive each term of the resulting expression is positive (the standard deviation parameters may be taken as positive without loss of generality). In that case, it is impossible that any term cancels with any other, so the resulting covariance is positive everywhere.

Last, we examine the recurrence relationship in equation 15. Once $\mathrm{Cov}(m^{(L-1)}_{ib}, m^{(L-1)}_{jd}) \neq 0$ for all possible indices, the covariances between elements of $M^{(L)}$ may also be non-zero. Observe simply that if the means of the top weight matrix are positive, then each of the terms in equation 15 are positive, so it is impossible for any term to cancel out with any other. The fact that the elements of $M^{(L-1)}$ have non-zero covariances everywhere therefore entails that there is a weight matrix $W^{(L)}$ such that $M^{(L)}$ has non-zero covariance between all of its elements also, as required.

Remark 3. *Here, we show only an existance proof, and therefore we restrict ourselves to positive means and standard deviations to simplify the proof. In fact, we believe that non-zero covariance is the norm, rather than a special case, and found this in all our numerical simulations for both trained and randomly sampled models. However, we do not believe that (in the linear case)* any *covariance matrix can be created from a deep mean-field product.*

□

D.2 Matrix Variate Gaussian as a Special Case of Three-Layer Product Matrix

We can gain insight into the richness of the possible covariances by considering the limited case of the product matrix $M^{(3)} = ABC$ where B is a matrix whose elements are independent Gaussian random variables and A and C are deterministic. We note that this is a highly constrained setting, and that the covariances which can be induced with A and C as random variables have the more complex form shown in D.1. We can show the following:

Proposition 2. *The Matrix Variate Gaussian (Kronecker-factored) distribution is a special case of the distribution over elements of the product matrix. In particular, for $M^{(3)} = ABC$, $M^{(3)}$ is distributed as an MVG random variable when A and C are deterministic and B has its elements distributed as fully factorized Gaussians with unit variance.*

Proof. Consider the product matrix $M^{(3)} = ABC$. where B is a matrix whose elements are independent Gaussian random variables and A and C are deterministic. The elements of B are distributed with mean μ_B and have a diagonal covariance matrix Σ_B.

We begin by recalling the property of the Kronecker product that:

$$\text{vec}(ABC) = (C^\top \otimes A)\text{vec}(B). \tag{20}$$

By definition $\text{vec}(M^{(3)}) = \text{vec}(ABC) = (C^\top \otimes A)\text{vec}(B)$. Because $C^\top \otimes A$ is deterministic, it follows from a basic property of the covariance that the covariance of the product matrix $\Sigma_{M^{(3)}}$ is given by:

$$\Sigma_{M^{(3)}} = (C^\top \otimes A)\Sigma_B(C^\top \otimes A)^\top. \tag{21}$$

Using the fact that the transpose is distributive over the Kronecker product, this is equivalent to:

$$\Sigma_{M^{(3)}} = (C^\top \otimes A)\Sigma_B(C \otimes A^\top). \tag{22}$$

Because we only want to establish that the family of distributions expressible contains the matrix variate Gaussians, we do not need to use all the possible freedom, and we can set $\Sigma_B = I$. In this special case:

$$\Sigma_{M^{(3)}} = (C^\top \otimes A)(C \otimes A^\top). \tag{23}$$

Using the mixed-product property, this is equivalent to:

$$\Sigma_{M^{(3)}} = (C^\top C) \otimes (AA^\top). \tag{24}$$

Now, we note that any positive semi-definite matrix can be written in the form $A = M^\top M$, so this implies that, defining the positive semi-definite matrices $V = C^\top C$ and $U = AA^\top$, we have that the covariance $\Sigma_{M^{(3)}}$ is of the form,

$$\Sigma_{M^{(3)}} = V \otimes U. \tag{25}$$

Similarly, we can consider the mean of the product matrix $\mu_{M^{(3)}}$. From equation 20, we can see that:

$$\mu_{M^{(3)}} = (C^\top \otimes A)\text{vec}(\mu_B). \tag{26}$$

But since we have not yet constrained μ_B, it is clear that this allows us to set any $\mu_{M^{(3)}}$ we desire by choosing $\mu_B = (C^\top \otimes A)^{-1}\mu_{M^{(3)}}$.

So far, we have only discussed the first- and second-moments, and the proof has made no assumptions about specific distributions. However, we now observe that a random variable X is distributed according to the Matrix Variate Gaussian distribution according to some mean μ_X and with scale matrices U and V if and only if $\text{vec}(X)$ is a multivariate Gaussian with mean $\vec{\mu_X}$ and covariance $U \otimes V$.

Therefore, given equations (26) and (25), the special case of $M^{(3)}$ where the first and last matrices are deterministic and the middle layer has a fully-factorized Gaussian distribution over the weights with unit variance is a Matrix Variate Gaussian distribution where:

$$\text{vec}(\mu_X) = (C^\top \otimes A)\text{vec}(\mu_B); \tag{27}$$

$$V = C^\top C; \tag{28}$$

$$U = A^\top A. \tag{29}$$

□

D.3 Distribution of the Product Matrix

In general the probability density function of a product of random variables is not the product of their density functions. In the scalar case, the product of two independent Gaussian distributions is a generalized χ^2 distribution. The product of arbitrarily many Gaussians with arbitrary non-i.i.d. mean and variance is difficult to calculate (special cases are much better understood e.g., Springer and Thompson [1970]). An example of a distribution family that *is* closed under multiplication is the log-normal distribution.

In the case of matrix multiplication, important for neural network weights, because each element of a product of matrix multiplication is the sum of the product of individual elements we would ideally like a distribution to be closed under both addition and multiplication (such as the Generalized Gamma convolution [Bondesson, 2015]) but these are not practical.

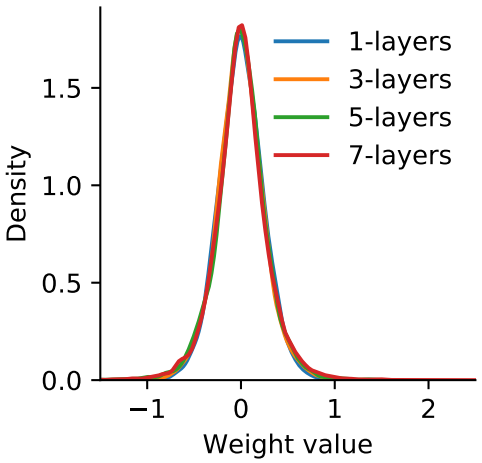

Figure 10: Density over arbitrary element of product matrix for L diagonal prior Gaussian weight matrices whose elements are i.i.d. $\mathcal{N}(0, 0.23^2)$. Product matrix elements are not strictly Gaussian, but very close.

Instead, it would be helpful if we could make use of a simple distribution like the Gaussian but maintain roughly similar distributions over product matrix elements as the network becomes deeper. For only one layer of hidden units, provided K is sufficiently large, we can use the central limit theorem to show that the elements of the product matrix composed of i.i.d. Gaussian priors tends to a Gaussian as the width of the hidden layer increases. For two or more layers, however, the central limit theorem fails because the elements of the product matrix are no longer independent. However, even though the resulting product matrix is not a Gaussian, we show through numerical simulation that products of matrices with individual weights distributed as $\mathcal{N}(0, 0.23^2)$ have roughly the same distribution over their weights. This, combined with the fact that our choice of Gaussian distributions over weights was somewhat arbitrary in the first place, might reassure us that the increase in depth does not change the model prior in an important way. In Figure 10 we plot the probability density function of an arbitrarily chosen entry in the product matrix with varying depths of diagonal Gaussian prior weights. The p.d.f. for 7 layers is approximately the same as the single-layer Gaussian distribution with variance 0.23^2.

D.4 Proof of Linearized Product Matrix Covariance

D.4.1 Proof of Local Linearity

We consider local linearity in the case of piecewise-linear activations like ReLU.

Lemma 1. *Consider an input point $\mathbf{x}^* \in \mathcal{D}$. Consider a realization of the model weights $\boldsymbol{\theta}$. Then, for any $\mathbf{x}^*$, the neural network function $f_{\boldsymbol{\theta}}$ is linear over some compact set $\mathcal{A}_{\boldsymbol{\theta}} \subset \mathcal{D}$ containing $\mathbf{x}^*$. Moreover, $\mathcal{A}_{\boldsymbol{\theta}}$ has non-zero measure for almost all $\mathbf{x}^*$ w.r.t. the Lebesgue measure.*

Proof. Neural networks with finitely many piecewise-linear activations are themselves piecewise-linear. Therefore, for a finite neural network, we can decompose the input domain $\mathcal{D}$ into regions $\mathcal{D}_i \subseteq \mathcal{D}$ such that

1. $\cup \mathcal{D}_i = \mathcal{D}$,
2. $\mathcal{D}_i \cap \mathcal{D}_j = \varnothing \quad \forall i \neq j$,
3. $f_{\boldsymbol{\theta}}$ is a linear function on points in $\mathcal{D}_i$ for each i.

For a finite neural network, there are at most finitely many regions $\mathcal{D}_i$. In particular, with hidden layer widths n_i in the i'th layer, with an input domain $\mathcal{D}$ with dimension n_0, Montúfar et al. [2014] show that the network can define maximally a number of regions in input space bounded above by:

$$\left(\prod_{i=1}^{L-1} \left\lfloor \frac{n_i}{n_0} \right\rfloor^{n_0}\right) \sum_{j=0}^{n_0} \binom{n_L}{j}. \tag{30}$$

Except in the trivial case where the input domain has measure zero, this along with (1) and (2) jointly entail that at least one of the regions $\mathcal{D}_i$ has non-zero measure. This, with (3) entails that only a set of input points of zero measure do *not* fall in a linear region of non-zero measure. These points correspond to inputs that lie directly on the inflection points of the ReLU activations. □

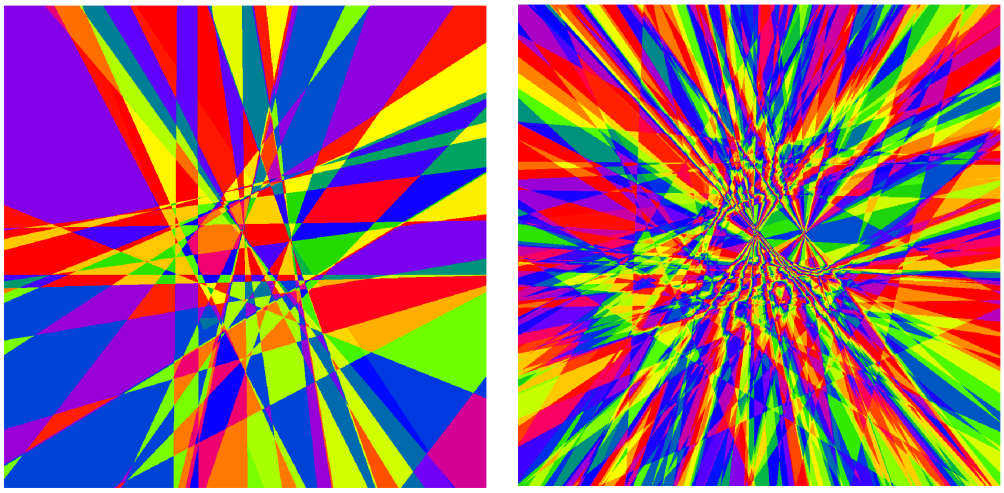

(a) 1 sample: $\mathcal{A}_{\boldsymbol{\theta}_i}$

(b) 5 samples: $\mathcal{A} = \bigcap_{0 \leq i < 5} \mathcal{A}_{\boldsymbol{\theta}_i}$

Figure 11: Visualizaton of the linear regions in input-space for a two-dimensional binary classification problem (two moons). Colored regions show contiguous areas within which a neural network function is linear. We use an abitrary numerical encoding of these regions (we interpret the sign pattern of activated relus as an integer in base 2) and a cylic colour scheme for visualisation, so the color of each region is arbitrary, and two non-contiguous regions with the same color are not the same region. The neural network has one hidden layer with 100 units and is trained for 1000 epochs on 500 datapoints from scipy's two moons using Adam. (a) a single model has fairly large linear regions, with the most detail clustered near the region of interest. (b) The regions within which all samples are linear (the intersection set $\mathcal{A}$) are smaller, but finite. The local product matrix is valid within one of these regions for any input point.

We visualize $\mathcal{A}_{\boldsymbol{\theta}_i}$ in Figure 11a. This shows a two-dimensional input space (from the two moons dataset). Parts of the space within which a neural network function is linear are shown in one color. The regions are typically smallest where the most detail is required in the trained function.

D.4.2 Defining the Local Product Matrix

We define a random variate representing the local product matrix, for an input point $\mathbf{x}^*$, using the following procedure.

To draw a finite N samples of the random variate, we sample N realizations of the weight parameters $\Theta = \{\boldsymbol{\theta}_i \text{ for } 1 \leq i \leq N\}$. For each $\boldsymbol{\theta}_i$, given $\mathbf{x}^*$ there is a compact set $\mathcal{A}_{\boldsymbol{\theta}_i} \subset \mathcal{D}$ within which $f_{\boldsymbol{\theta}_i}$ is linear (and $\mathbf{x}^* \in \mathcal{A}_i$) by lemma 1. Therefore, all samples of the neural network function are linear in the intersection region $\mathcal{A} = \bigcap_i \mathcal{A}_{\boldsymbol{\theta}_i}$. We note that $\mathcal{A}$ at least contains $\mathbf{x}^*$. Moreover, so long as $\mathcal{D}$ is a compact subset of the reals, $\mathcal{A}$ has non-zero measure.[6] Figure 11b shows a visualization of $\mathcal{A}$ with 5 samples. The linear regions are smaller, because there is a discontinuity if any of the models is

[6]Intuitively, we know that $\mathbf{x}^*$ is in all $\mathcal{A}_{\boldsymbol{\theta}_i}$, so when we add a new sample we know that there is either overlap around $\mathbf{x}^*$ or the point $\mathbf{x}^*$ is on the boundary of the new subset, which means we could equally well pick a different set that has $\mathbf{x}^*$ on its boundary and *does* have non-zero-measure overlap with the previous sets.

More formally, consider some compact set $\mathcal{A}_{\boldsymbol{\theta}_0} \subset \mathcal{D}$ with non-zero measure such that $\mathbf{x}^* \in \mathcal{A}_{\boldsymbol{\theta}_0}$. Take some new compact set $\mathcal{A}_{\boldsymbol{\theta}_1} \subset \mathcal{D}$ with non-zero measure also such that $\mathbf{x}^* \in \mathcal{A}_{\boldsymbol{\theta}_1}$. Define the intersection between those sets $\mathcal{B} = \mathcal{A}_{\boldsymbol{\theta}_0} \cap \mathcal{A}_{\boldsymbol{\theta}_1}$. Suppose that $\mathcal{B}$ has zero measure. But both $\mathcal{A}_{\boldsymbol{\theta}_0}$ and $\mathcal{A}_{\boldsymbol{\theta}_1}$ contain $\mathbf{x}^*$, so the only way that $\mathcal{B}$ could have zero measure is if $\mathbf{x}^*$ is an element in the boundary of both sets. But if $\mathcal{A}_{\boldsymbol{\theta}_1}$ has $\mathbf{x}^*$ on its boundary, then, by the continuity of the real space, there is at least one other compact set $\mathcal{A}'_{\boldsymbol{\theta}_1}$, different to $\mathcal{A}_{\boldsymbol{\theta}_1}$, such that $\mathbf{x}^*$ is on its boundary. But, since by hypothesis $\mathcal{A}_{\boldsymbol{\theta}_0}$ has non-zero measure, there exists such a set $\mathcal{A}'_{\boldsymbol{\theta}_1}$ which has a non-zero-measure intersection with $\mathcal{A}_{\boldsymbol{\theta}_0}$. We can therefore select $\mathcal{A}'_{\boldsymbol{\theta}_1}$ instead of $\mathcal{A}_{\boldsymbol{\theta}_1}$ when building $\mathcal{A}$, such that the intersection with $\mathcal{A}_{\boldsymbol{\theta}_0}$ has non-zero measure. By repeated application of this argument, we can guarantee that for any finite Θ we are able to find a set of $\mathcal{A}_{\boldsymbol{\theta}_i} \subset \mathcal{D}$ such that $\forall i : \mathbf{x}^* \in \mathcal{A}_{\boldsymbol{\theta}_i}$ and $\mathcal{A}$ has non-zero measure. This argument does not guarantee that the measure of $\mathcal{A}$ in the limit as N tends to infinity is non-zero.

discontinuous. Nevertheless, the space is composed of regions of finite size within which the neural network function is linear.

For each $\boldsymbol{\theta}_i$ we can compute a local product matrix within $\mathcal{A}$. Ordinarily, setting aside the bias term for simplicity, a neural network hidden layer $\mathbf{h}_{l+1}$ can be written in terms of the hidden layer before it, a weight matrix W_l, and an activation function.

$$\mathbf{h}_{l+1} = \sigma(W_l \mathbf{h}_l) \tag{31}$$

We observe that within $\mathcal{A}$ the activation function becomes linear. This allows us to define an activation vector $\mathbf{a}_{\mathbf{x}^*}$ within $\mathcal{A}$ such that the equation can be written:

$$\mathbf{h}_{l+1} = \mathbf{a}_{\mathbf{x}^*} \cdot (W_l \mathbf{h}_l). \tag{32}$$

The activation vector can be easily calculated by calculating $W_l \mathbf{h}_l$, seeing which side of the (Leaky) ReLU the activation is on within that linear region for each hidden unit, and selecting the correct scalar (0 or 1 for a ReLU, or α or 1 for a Leaky ReLU).

This allows us to straightforwardly construct a product matrix for each $\boldsymbol{\theta}_i$ which takes the activation function into account (in the linear case, we effectively always set $\mathbf{a}_{\mathbf{x}^*}$ to equal the unit vector). The random variate $P_{\mathbf{x}^*}$ is constructed with these product matrices for realizations of the weight distribution.

Samples from the resulting random variate $P_{\mathbf{x}^*}$ are therefore distributed such that samples from $P_{\mathbf{x}^*}\mathbf{x}^*$ have the same distribution as samples of the predictive posterior y given $\mathbf{x}^*$ within $\mathcal{A}$.

D.4.3 Proof that the Local Product Matrix has Non-zero Off-diagonal Covariance

Proposition 3. *Given a mean-field distribution over the weights of neural network f with piecewise linear activations, f can be written in terms of the local product matrix $P_{\mathbf{x}^*}$ within $\mathcal{A}$.*

For $L \geq 3$, for activation functions which are non-zero everywhere, there exists a set of weight matrices $\{W^{(l)} | 1 \leq l < L\}$ such that all elements of the local product matrix have non-zero off-diagonal covariance:

$$\text{Cov}(p_{ab}^{\mathbf{x}^*}, p_{cd}^{\mathbf{x}^*}) \neq 0, \tag{2}$$

where $p_{ij}^{\mathbf{x}^*}$ is the element at the i^{th} row and j^{th} column of $P_{\mathbf{x}^*}$.

Proof. First, we show that the covariance between arbitrary entries of each realization of the product matrix of linearized functions can be non-zero. Afterwards, we will show that this implies that the covariance between arbitrary entries of the product matrix random variate, $P_{\mathbf{x}^*}$ can be non-zero.

Consider a local product matrix constructed as above. Then for each realization of the weight matrices, the product matrix realization $M_i^{(L)}$, defined in the region around $\mathbf{x}^*$ following lemma 1. We can derive the covariance between elements of this product matrix within that region in the same way as in Proposition 1, finding similarly that:

$$\begin{aligned}
\hat{\Sigma}^{(3)}_{abcd} = \alpha_{abcd} \sum_{ij} \left(\delta_{ac} \delta_{ij} \sigma^{(3)}_{ai} \right) \cdot \sum_k \Big(& \delta_{ij} \delta_{bd} \sigma^{(2)}_{ik} \sigma^{(1)}_{kb} \\
& + \delta_{bd} \mu^{(2)}_{ik} \mu^{(2)}_{jk} \sigma^{(1)}_{kb} \\
& + \delta_{ij} \mu^{(1)}_{kb} \mu^{(1)}_{kd} \sigma^{(2)}_{ik} \Big) \\
+ \mu^{(3)}_{ai} \mu^{(3)}_{cj} \cdot \sum_k \Big(& \delta_{ij} \delta_{bd} \sigma^{(2)}_{ik} \sigma^{(1)}_{kb} \\
& + \delta_{bd} \mu^{(2)}_{ik} \mu^{(2)}_{jk} \sigma^{(1)}_{kb} \\
& + \delta_{ij} \mu^{(1)}_{kb} \mu^{(1)}_{kd} \sigma^{(2)}_{ik} \Big) \\
+ \mu^{(2)}_{ib} \mu^{(2)}_{jd} \left(\delta_{ac} \delta_{ij} \sigma^{(3)}_{ai} \right), &
\end{aligned} \tag{33}$$

where α is a constant determined by the piecewise-linearity in the linear region we are considering. Note that we must assume here that $\alpha_{ij} \neq 0$ except in a region of zero measure, for example a LeakyReLU, otherwise it is possible that the constant introduced by the activation could eliminate non-zero covariances. We discuss this point further below.

Now note that the covariance of the sum of independent random variables is the sum of their covariances. Therefore the covariance of I realizations of P (suppressing the notation (L)) is:

$$\mathrm{Cov}\big(P_{ab}, P_{cd}\big) = \frac{1}{I}\sum_{i=1}^{I} \hat{\Sigma}^{i}_{abcd} \tag{34}$$

As before, consider the case of positive means and standard deviations. Just like before, this results in a positive entry in the covariance between any two elements for each realization of the product matrix, and by equation 34 the entry for any element of the local product matrix remains positive as well. This suffices to prove the proposition for the case of $L = 3$. Just as Proposition 1 extends to all larger L, this result does also.

Remark 4. *The above proof assumes that $\alpha_{ij} \neq 0$. In fact, for common piecewise non-linearities like ReLU, α may indeed be zero. This means that the non-linearity can, in principle, 'disconnect' regions of the network such that the 'effective depth' falls below 3 and there is not a covariance between every element.*

We cannot rule this out theoretically, as it depends on the data and learned function. In practice, we find it very unlikely that a trained neural network will turn off all its activations for any typical input, nor that enough activations will be zero that the product matrix does not have shared elements after some depth.

However, we do observe that for at least some network structures and datasets it is uncommon in practice that all the activations in several layers are 'switched off'. We show in Figure 1 an example of a local product matrix covariance which does not suffer from this problem. We find that for a model trained with mean-field VI on the FashionMNIST test dataset the number of activations switched on is on average 48.5% with standard deviation 4.7%. There were only four sampled models out of 100 samples on each of 10,000 test points where an entire row of activations was 'switched off', reducing the effective depth by one, and this never occurred in more than one row. Indeed, [Goldblum et al., 2019] describe settings with all activations switched off as a pathological case where SGD fails.

□

D.5 Existence Proof of a Two-Hidden-Layer Mean-field Approximate Posterior Inducing the True Posterior Predictive

In this section we prove that:

Proposition 4. *Let $p(\mathbf{y} = \mathbf{Y}|\mathbf{x}, \mathcal{D})$ be the probability density function for the posterior predictive distribution of any given multivariate regression function, with $\mathbf{x} \in \mathbb{R}^D$, $\mathbf{y} \in \mathbb{R}^K$, and $\mathbf{Y}$ the posterior predictive random variable. Let $f(\cdot)$ be a Bayesian neural network with two hidden layers. Let $\hat{\mathbf{Y}}$ be the random vector defined by $f(\mathbf{x})$. Then, for any $\epsilon, \delta > 0$, there exists a set of parameters defining the neural network f such that the absolute value of the difference in probability densities for any point is bounded:*

$$\forall \mathbf{y}, \mathbf{x}, i: \quad \Pr\Big(|p(y_i = \hat{Y}_i) - p(y_i = Y_i|\mathbf{x}, \mathcal{D})| > \epsilon\Big) < \delta, \tag{3}$$

so long as: the activations of f are non-polynomial, non-periodic, and have only zero-measure non-monotonic regions, the first hidden layer has at least $D + 1$ units, the second hidden layer has an arbitrarily large number of units, the cumulative density function of the posterior predictive is continuous in output-space, and the probability density function is continous and finite non-zero everywhere. Here, the probability bound is with respect to the distribution over a subset of the weights described in the proof, $\boldsymbol{\theta}_{\mathrm{Pr}}$, while one weight distribution $\boldsymbol{\theta}_Z$ remains to induce the random variable $\hat{\mathbf{Y}}$.

Proof. We extend an informal construction by Gal [2016] which aimed to show that a sufficiently deep network with a unimodal approximate posterior could induce a multi-modal posterior predictive

by learning the inverse cumulative distribution function (c.d.f.) of the multi-modal distribution. In our case, we are not chiefly interested in the number of modes, but more generally the expressive power of the mean-field distribution in a BNN of sufficient width and depth. First, we outline a simplified version of the proof that highlights the main mechanisms involved but is not constructed with a Bayesian neural network. Later, we prove the full result for Bayesian neural networks.

D.5.1 Simplified Construction

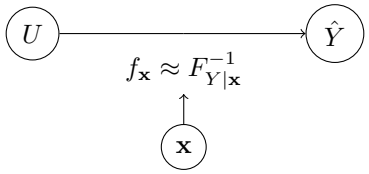

Figure 12: The random variable whose probability density function is the true predictive posterior $p(y|\mathbf{x}, \mathcal{D})$ can be written $Y|\mathbf{x}$. If it has an inverse cumulative density function (c.d.f.), $F^{-1}_{Y|\mathbf{x}}$, we can transform a uniform random variable U onto it. We can approximate this inverse c.d.f. with $f_{\mathbf{x}}$ indexed by $\mathbf{x}$. The random variable given by $\hat{Y} \coloneqq f_{\mathbf{x}}(U)$ can be constructed to be 'similar' to $Y|\mathbf{x}$ as we show.

Lemma 2. *Let $p(y = Y|\mathbf{x}, \mathcal{D})$ be the probability density function for the posterior predictive distribution of any given univariate regression function. Let U be a uniformly distributed random variable. Let $f(\cdot)$ be a deterministic neural network with a single hidden layer of arbitrary width and invertible non-polynomial activations. Let $\hat{Y}$ be the random variable defined by $f(U, \mathbf{x})$. Then, for any $\epsilon > 0$, there exists a set of parameters defining a sufficiently wide f such that the absolute value of the difference in probability densities for any point is bounded:*

$$\forall y, \mathbf{x}: \quad |p(y = \hat{Y}) - p(y = Y|\mathbf{x}, \mathcal{D})| < \epsilon, \tag{35}$$

so long as the cumulative distribution function of the posterior predictive is continuous in output-space and the probability density function is non-zero everywhere.

Proof. An outline of the proof for the simplified case is shown in Figure 12.

Suppose there is a true posterior distribution over function outputs whose probability density function (p.d.f) is given by $p(y = Y|\mathbf{x}, \mathcal{D})$. These define a random variable that we will denote $Y|\mathbf{x}$.

We also have some approximation that takes $\mathbf{x}$ as an input and returns some y in the output space. Later, this will be our Bayesian neural network, but for now we simplify. Instead, our procedure is to have some deterministic neural network which accepts as an input a realization of a uniformly distributed random variable, U, and the input point $\mathbf{x}$. We define a random variable $\hat{Y} \coloneqq f(U, \mathbf{x})$.

We would like to show that it is possible to construct a neural network f such that the result in equation (35) holds—that $\hat{Y}$ is suitably similar to the true predictive posterior random variable $Y|\mathbf{x}$.

First, note that if $Y|\mathbf{x}$ has an inverse cumulative density function (c.d.f.) then, by the universality of the uniform, transforming a uniform random variable by this function creates a random variable distributed as $Y|\mathbf{x}$. As a result, if there is such an invertible cumulative density function, there is also a function mapping U and $\mathbf{x}$ onto $Y|\mathbf{x}$.

Second, consider the conditions under which $Y|\mathbf{x}$ has an invertible c.d.f. We must assume that the c.d.f. is continuous in output space and that the probability density function is non-zero everywhere. The first is reasonable for most normal problems, we often make a stronger assumption of Lipschitz continuity. The second is also relatively mild, corresponding to non-dogmatic certainty (a posterior distribution that puts zero probability density on some output given some input can never update away from that in light of new information). Given these mild assumptions, therefore, we know that there exists a continuous function $F^{-1}_{Y|\mathbf{x}}$ which is the inverse of the c.d.f. of $Y|\mathbf{x}$.

Third, we consider how we might approximate this function. Here, we invoke the universal approximation theorem (UAT) [Leshno et al., 1993]. This states that for any continuous function g, arbitrary

fixed error, ϵ, and compact subset $\mathcal{A}$ of $\mathbb{R}^D$, there exists a deterministic neural network with an arbitrarily wide single layer of hidden units and a non-polynomial activation, f such that:

$$\forall \mathbf{a} \in \mathcal{A} : |f(\mathbf{a}) - g(\mathbf{a})| < \epsilon. \tag{36}$$

By setting the arbitrary continuous function as the inverse c.d.f. of $Y|\mathbf{x}$, that is, $g(U, \mathbf{x}) = F^{-1}_{Y|\mathbf{x}}(U)$ (which we have already assumed is continuous) it follows that:

$$\forall u, \mathbf{x} \in \mathcal{A} : |f(u, \mathbf{x}) - F^{-1}_{Y|\mathbf{x}}(u)| < \epsilon, \quad u \sim U. \tag{37}$$

Fourth, we convert this bound on the inverse c.d.f. into a bound on the c.d.f. and then a bound on the p.d.f. We rewrite the function represented by the neural network to make explicit that we are using $\mathbf{x}$ to index a function from u to y: $y = f(u, \mathbf{x}) = f_{\mathbf{x}}(u)$.

For this step, we will need to be able to invert the approximation to the inverse CDF such that $u = f^{-1}_{\mathbf{x}}(y)$ (for fixed $\mathbf{x}$). In general for neural network functions this is not true. As a result, we employ a construction which breaks apart the line over which y runs into subsegments within which the network is invertible. For non-periodic activation functions which have only zero-measure non-monotonic regions (e.g., ReLU) there will be finitely many of these segments given a finite number of hidden units. Let us index over these subregions with i, noting that we can think of the distribution over y as a weighted mixture distribution whose members have zero-density outside of the subregions. The approximate inverse CDF of each of these sub-region mixture members can be written as $f^i_{\mathbf{x}}(u)$ such that $f_{\mathbf{x}}(u) = \sum_i f^i_{\mathbf{x}}(u)$. Each of these $f^i_{\mathbf{x}}(u)$ is invertible. We can therefore rewrite equation (37) as:

$$\forall y, \mathbf{x} \in \mathcal{A} : \quad |\sum_i f_{\mathbf{x}}({f^i_{\mathbf{x}}}^{-1}(y)) - F^{-1}_{Y|\mathbf{x}}({f^i_{\mathbf{x}}}^{-1}(y))| < \epsilon. \tag{38}$$

which implies that:

$$\forall y, \mathbf{x} \in \mathcal{A} : \quad |\sum_i y - F^{-1}_{Y|\mathbf{x}}({f^i_{\mathbf{x}}}^{-1}(y))| < \epsilon. \tag{39}$$

Remember that we assumed above that the c.d.f. of $Y|\mathbf{x}$ is uniformly continuous, which means that for any y' and y'', and any $\epsilon > 0$ there exists a δ such that if $|y' - y''| < \delta$ then $|F_{Y|\mathbf{x}}(y') - F_{Y|\mathbf{x}}(y'')| < \epsilon$. Alongside equation (39), and canceling the c.d.f. with the inverse c.d.f. this entails that:

$$\forall y, \mathbf{x} \in \mathcal{A} : \quad |\sum_i F_{Y|\mathbf{x}}(y) - {f^i_{\mathbf{x}}}^{-1}(y))| < \epsilon. \tag{40}$$

But since ${f^i_{\mathbf{x}}}^{-1}(y)$ is zero by construction outside of its subregion, this results in a bound on the overall c.d.f. of the random variable. That is to say, the bound on the inverse c.d.f. implies a bound on the c.d.f.

Finally, we remember that the cumulative density is the integral of the probability density function. Therefore, by Theorem 7.17 of Rudin [1976] and the uniform convergence in the c.d.f.s, it follows that:

$$\forall y, \mathbf{x} \in \mathcal{A} : \quad |p(y = Y|\mathbf{x}, \mathcal{D}) - p(y = \hat{Y})| < \epsilon \tag{41}$$

introducing a bound in the probability density functions of the random variable of true posterior outputs and the outputs of the approximation $\hat{Y} = f(U, \mathbf{x})$. □

D.5.2 Full Construction

The full construction extends the result above in the following ways:

- Rather than separately introducing U, we show how the first layer of a Bayesian neural network can map $\mathbf{x} \to \mathbf{x}', Z$, where Z is a unit Gaussian random variable and $\mathbf{x}'$ is a noised version of $\mathbf{x}$.
- Rather than using a deterministic neural network for the universal approximation theorem, we apply the stochastic adaptation introduced by Foong et al. [2020].
- Rather than a univariate regression, we consider multivariate regression.

Like Leshno et al. [1993] we note that the extension from univariate to multivariate regression follows trivially from the existence of a mapping from $\mathbb{R} \to \mathbb{R}^K$.[7]

We first give some intuition as to how the proof works. The first weight layer serves to map $\mathbf{x} \to \mathbf{x}', Z$. This sets us up in a similar situation to the proof in the previous section, where we began with $\mathbf{x}, U$. This requires two small adjustments to the proof above. The first is that the random variable we introduce is now Gaussian, rather than Uniform. The second is that all our results will be in terms of $\mathbf{x}'$, rather than $\mathbf{x}$, and an additional step will be required to convert a probabilistic bound in one to the other (noting that we can freely set the weights in the first layer to have arbitrarily small variance).

The second weight layer will play the role of the neural network in the simplified proof. This also will require a small modification, because earlier we assumed that the neural network was deterministic, but it is now stochastic. This means that the final result becomes a probabilistic bound.

As a result of all of these changes, the proof becomes considerably more complicated, though nothing important changes in the intuition behind the construction.

Step 1: Mapping $\mathbf{x} \to \mathbf{x}', Z$

Consider inputs $\mathbf{x} \in \mathbb{R}^D$. We define a two-hidden-layer neural network with an invertible non-polynomial activation function $\phi : \mathbb{R} \mapsto \mathbb{R}$. The first component of the network is a single weight matrix mapping onto a vector of hidden units: $\mathbf{h}_1 = \phi(\boldsymbol{\theta}_0\mathbf{x} + \mathbf{b}_0)$. The second component is a neural network with a layer of hidden units defined relative to the first layer of units $\mathbf{h}_2 = \phi(\boldsymbol{\theta}_1\mathbf{h}_1 + \mathbf{b}_1)$, and outputs $\mathbf{y} = \boldsymbol{\theta}_2\mathbf{h}_2 + \mathbf{b}_2$. The distribution over the outputs $\mathbf{y}$ defines the random variable $\hat{\mathbf{Y}}$. Here, $\boldsymbol{\theta}_0$, $\boldsymbol{\theta}_1$, and $\boldsymbol{\theta}_2$ are matrices of independent Gaussian random variables and $\mathbf{b}_0$, $\mathbf{b}_1$, and $\mathbf{b}_2$ are vectors of independent Gaussian random variables. Given some dataset $\mathcal{D}$ the predictive posterior distribution over outputs is $p(\mathbf{y}|\mathbf{x}, \mathcal{D})$ which we associate with the random variable $\mathbf{Y}$. This is our (intractable) target.

Consider only the first component of the neural network, which maps $\mathbf{x}$ onto $\mathbf{h}_1$. We can construct simple constraints on $\boldsymbol{\theta}_0$ and $\mathbf{b}_0$ such that:

$$\mathbf{h}_1 = \begin{pmatrix} \phi(z) \\ \phi(\mathbf{x}') \end{pmatrix}, \tag{42}$$

where $z \sim Z$, a unit Gaussian random variable, and $\mathbf{x}' \in \mathbb{R}^D$, such that $\Pr\left(\|\mathbf{x}' - \mathbf{x}\| > \epsilon_1\right) < \delta_1$. In particular, suppose that for $\boldsymbol{\theta}_0 \in \mathbb{R}^{D \times D+1}$ and $\mathbf{b}_0 \in \mathbb{R}^{D+1}$:

$$\boldsymbol{\theta}_0 = \mathcal{N}\left(M_{\boldsymbol{\theta}_0}, \Sigma_{\boldsymbol{\theta}_0}\right) \text{ where } M_{\boldsymbol{\theta}_0} = (\mathbf{0}_D, \mathbb{I}_{D \times D}); \Sigma_{\boldsymbol{\theta}_0} = \sigma^2 \mathbb{I}_{D \times D+1}; \tag{43}$$

$$\mathbf{b}_0 = \mathcal{N}\left(\boldsymbol{\mu}_{\mathbf{b}_0}, \boldsymbol{\sigma}_{\mathbf{b}_0}\right) \text{ where } \boldsymbol{\mu}_{\mathbf{b}_0} = \mathbf{0}_{D+1}, \boldsymbol{\sigma}_{\mathbf{b}_0} = \begin{pmatrix} 1 & \sigma & \dots & \sigma \end{pmatrix}. \tag{44}$$

By multiplication, straightforwardly $\mathbf{x}' = \mathcal{N}\left(\mathbf{x}, 2\sigma^2\mathbf{1}\right)$. It follows trivially that for any ϵ_1 and δ_1 there exists some σ such that the bound holds. We will apply this bound at the end of the proof to convert a bound in $\mathbf{x}'$ to one in $\mathbf{x}$.

Here, we introduce a distinction between the weights which determine $\mathbf{x}'$ and those that create Z. The only weights which determine Z are the first element of $\boldsymbol{\theta}_0$ and the first element of $\mathbf{b}_0$. Call these $\boldsymbol{\theta}_Z$. We then define the remainder of the weight distributions as $\boldsymbol{\theta}_{\text{Pr}} \coloneqq \{\boldsymbol{\theta}_0, \boldsymbol{\theta}_1, \boldsymbol{\theta}_2, \mathbf{b}_0, \mathbf{b}_1, \mathbf{b}_2\} \setminus \boldsymbol{\theta}_Z$. This distinction is important, because the probabilistic bound in the proof will be over $\boldsymbol{\theta}_{\text{Pr}}$ while the distribution over $\boldsymbol{\theta}_Z$ will induce the random variable $\hat{\mathbf{Y}}$.

Step 2: Invoking a Result Similar to the Simplified Construction

We show that there is a function which maps Z and $\mathbf{x}'$ onto $\mathbf{Y}$, under reasonable assumptions similar to those of the simplified construction. For brevity, we denote the probability density function (p.d.f.) of the true posterior predictive distribtion of the random variable $\mathbf{Y}$ conditioned on $\mathbf{x}'$ and $\mathcal{D}$ as $f_{Y|\mathbf{x}'} \equiv p(Y = y|\mathbf{x}', \mathcal{D})$ and the cumulative density function (c.d.f.) as $F_{Y|\mathbf{x}'}$. We similarly write the inverse c.d.f. as $F^{-1}_{Y|\mathbf{x}'}$.

We must adapt the simplified construction to account for the fact that rather than simply approximating the inverse of the c.d.f. we now need to also transform the Gaussian random variable onto a Uniform one and invert the activation. We show below:

[7] A slightly complication is added by the continuity requirements. However, we note that the assumption that the p.d.f. is finite everywhere guarantees that there is a continuous function over y which contains continous segments for each of K dimensions, even if those individual segments are not continuous with each other.

Lemma 3. *There exists continous function $G^{-1}_{\mathbf{x}'} = F^{-1}_{Y|\mathbf{x}'} \cdot F_Z \cdot \phi^{-1}$, where F_Z is the c.d.f. of the unit Gaussian and ϕ^{-1} is the inverse of the activation function, such that the random variable $G^{-1}_{\mathbf{x}'}(\phi(Z))$ is equal in distribution to $\mathbf{Y}|\mathbf{x}$, if the p.d.f. of the posterior predictive is non-zero everywhere and the c.d.f. is continuous.*

The limitation to p.d.f.s is modest as before. The naming of the function $G^{-1}_{\mathbf{x}'}$ is suggestive, and indeed its inverse exists if $F_{Y|\mathbf{x}'}$ is invertible, since the c.d.f. of a unit Gaussian is invertible (though this function cannot be easily expressed).

Whereas in the simplified construction we showed that the neural network could approximate the inverse c.d.f., here we show that the second hidden layer of our larger Bayesian neural network can approximate the more complicated function required by lemma 3. This allows the second hidden layer of the neural network to transform $\mathbf{x}', Z$ onto $\hat{\mathbf{Y}}$ such that $\hat{\mathbf{Y}}$ is appropriately similar to $\mathbf{Y}$. First we show that we can approximate the function $G^{-1}_{\mathbf{x}'}$, generating a probabilistic bound because the weights of the neural network are now Gaussian random variables:

Lemma 4. *For a uniformly continous function $G^{-1}_{\mathbf{x}'}(z) : z, \mathbf{x}' \mapsto \mathbf{y}$, for any $\epsilon, \delta > 0$ and compact subset $\mathcal{A}$ of $\mathbb{R}^D$, there exist fully-factorized Gaussian approximating distributions $q(\boldsymbol{\theta}_1)$, $q(\boldsymbol{\theta}_2)$, $q(\mathbf{b}_1)$, and $q(\mathbf{b}_2)$, and a function over the outputs of the later part of the neural network: $\hat{G}^{-1}(\mathbf{x}', z) \equiv \boldsymbol{\theta}_2(\sigma(\boldsymbol{\theta}_1\mathbf{h}_1) + \mathbf{b}_1) + \mathbf{b}_2$ (remembering that $\mathbf{h}_1 \equiv \phi(z, \mathbf{x}')$), such that:*

$$\Pr\Big(\big|\hat{G}^{-1}(\mathbf{x}', z) - G^{-1}_{\mathbf{x}'}(z)\big| > \epsilon\Big) < \delta, \quad \forall \mathbf{x}' \in \mathcal{A}, z. \tag{45}$$

The probability measure is over the weight distributions of $\boldsymbol{\theta}_1, \boldsymbol{\theta}_2, \mathbf{b}_1, \mathbf{b}_2$.

Having shown that the second component can approximate the inverse c.d.f. to within a bound, we as before we further show that the random variable created by this transformation has a p.d.f. within a bound of the p.d.f. of $\mathbf{Y}$, which suffices to prove the desired result.

For this, we show this below for the transformed variable $\mathbf{x}'$:

Lemma 5. *For any $\epsilon > 0$ and $\delta > 0$ there exists a mean-field weight distribution $q(\boldsymbol{\theta}_1, \boldsymbol{\theta}_2, \mathbf{b}_1, \mathbf{b}_2)$ such that the probability density functions are bounded:*

$$\Pr\Big(\big|p(y_i = \hat{\mathbf{Y}}_i) - p(y_i = \mathbf{Y}_i|\mathbf{x}', \mathcal{D})\big| > \epsilon\Big) < \delta, \quad \forall \mathbf{x}', y_i, \mathcal{A}. \tag{46}$$

We then move the bounds onto an expression in the original features, $\mathbf{x}$. Recall from before that because the variance of the weights in the first layer can be arbitrarily small, that for any ϵ there is a δ:

$$\Pr\left(\|\mathbf{x}' - \mathbf{x}\| > \epsilon\right) < \delta \quad \forall \mathbf{x}, \mathbf{x}' \in \mathcal{A}, \tag{47}$$

where the probability measure is over $\boldsymbol{\theta}_{\text{Pr}}$. Moreover, since we have assumed that the probability density function is continuous, this bound alongside the previous bound on the probability density functions jointly entail that:

$$\Pr\Big(\big|p(y_i = \hat{\mathbf{Y}}_i) - p(y_i = \mathbf{Y}_i|\mathbf{x}, \mathcal{D})\big| > \epsilon\Big) < \delta, \quad \forall \mathbf{x} \in \mathcal{A}, y_i. \tag{48}$$

where the probability measure is over $\boldsymbol{\theta}_{\text{Pr}}$.

□

Below, we prove the lemmas required in the proposition above.

Lemma 3. *There exists continous function $G^{-1}_{\mathbf{x}'} = F^{-1}_{Y|\mathbf{x}'} \cdot F_Z \cdot \phi^{-1}$, where F_Z is the c.d.f. of the unit Gaussian and ϕ^{-1} is the inverse of the activation function, such that the random variable $G^{-1}_{\mathbf{x}'}(\phi(Z))$ is equal in distribution to $\mathbf{Y}|\mathbf{x}$, if the p.d.f. of the posterior predictive is non-zero everywhere and the c.d.f. is continuous.*

Proof. Trivially $\phi^{-1}(\phi(Z)) = Z$.

Let F_Z be the cummulative distribution function (c.d.f.) of the unit Gaussian random variable Z. By the Universality of the Uniform, $U = F_Z(Z)$ has a standard uniform distribution.

Let $F_{Y|\mathbf{x}}$ be the c.d.f. of $\mathbf{Y}$ conditioned on $\mathbf{x}$, and $\mathcal{D}$. Suppose that the posterior predictive is non-zero everywhere (that is, you cannot rule out that there's even the remotest chance of any y_i given some input $\mathbf{x}$, however small). Then, since the c.d.f. is continuous by assumption, $F_{Y|\mathbf{x}}$ is invertible.

Again, by the Universality of the Uniform $U' = F_{Y|\mathbf{x}}(y)$ has a standard uniform distribution. So $\forall u : p(U = u) = p(U' = u)$. Moreover $F_{Y|\mathbf{x}}$ is invertible. So $p(Y = y) = F^{-1}_{Y|\mathbf{x}}(F_Z(Z))$.

It follows that there exists a continuous function as required.

□

Lemma 4. *For a uniformly continous function $G^{-1}_{\mathbf{x}'}(z) : z, \mathbf{x}' \mapsto \mathbf{y}$, for any $\epsilon, \delta > 0$ and compact subset $\mathcal{A}$ of $\mathbb{R}^D$, there exist fully-factorized Gaussian approximating distributions $q(\boldsymbol{\theta}_1)$, $q(\boldsymbol{\theta}_2)$, $q(\mathbf{b}_1)$, and $q(\mathbf{b}_2)$, and a function over the outputs of the later part of the neural network: $\hat{G}^{-1}(\mathbf{x}', z) \equiv \boldsymbol{\theta}_2(\sigma(\boldsymbol{\theta}_1\mathbf{h}_1) + \mathbf{b}_1) + \mathbf{b}_2$ (remembering that $\mathbf{h}_1 \equiv \phi(z, \mathbf{x}')$), such that:*

$$\Pr\Big(\big|\hat{G}^{-1}(\mathbf{x}', z) - G^{-1}_{\mathbf{x}'}(z)\big| > \epsilon\Big) < \delta, \quad \forall \mathbf{x}' \in \mathcal{A}, z. \tag{45}$$

The probability measure is over the weight distributions of $\boldsymbol{\theta}_1, \boldsymbol{\theta}_2, \mathbf{b}_1, \mathbf{b}_2$.

Proof. The Universal Approximation Theorem (UAT) states that for any continuous function f, and an arbitrary fixed error, e, and compact subset $\mathcal{A}$ of $\mathbb{R}^D$, there exists a deterministic neural network with an arbitrarily wide single layer of hidden units and a non-polynomial activation, σ:

$$\forall \mathbf{x} \in \mathcal{A} : |\sigma(\mathbf{w}_2(\sigma(\mathbf{w}_1\mathbf{x}) + \mathbf{b}_1) + \mathbf{b}_2) - f(\mathbf{x})| < e. \tag{49}$$

In addition, we make use of Lemma 7 of [Foong et al., 2020]. This states that for any $e', \delta_2 > 0$, for some fixed means $\boldsymbol{\mu}_1$, $\boldsymbol{\mu}_2$, $\boldsymbol{\mu}_{b_1}$, $\boldsymbol{\mu}_{b_2}$ of $q(\boldsymbol{\theta}_1)$, $q(\boldsymbol{\theta}_2)$, $q(\mathbf{b}_1)$, and $q(\mathbf{b}_2)$ respectively, there exists some standard deviation $s' > 0$ for all those approximate posteriors such that for all $s < s'$, for any $\mathbf{h}_1 \equiv (z, \mathbf{x}') \in \mathbb{R}^{N+1}$

$$\Pr\Big(\big|\sigma(\boldsymbol{\theta}_2(\sigma(\boldsymbol{\theta}_1\mathbf{h}_1) + \mathbf{b}_1) + \mathbf{b}_2) - \sigma(\boldsymbol{\mu}_2(\sigma(\boldsymbol{\mu}_1\mathbf{h}_1) + \boldsymbol{\mu}_{b_1}) + \boldsymbol{\mu}_{b_2})\big| > e'\Big) < d. \tag{50}$$

Note that the deterministic weights of equation (49) can just be these means. As a result:

$$\Pr\Big(\big|\sigma(\boldsymbol{\theta}_2(\sigma(\boldsymbol{\theta}_1\mathbf{h}_1) + \mathbf{b}_1) + \mathbf{b}_2) - f(\mathbf{h}_1)\big| > e + e'\Big) < \delta. \tag{51}$$

We note that we define $\hat{G}^{-1}(\mathbf{x}', z) \equiv \sigma(\boldsymbol{\theta}_2(\sigma(\boldsymbol{\theta}_1\mathbf{h}_1) + \mathbf{b}_1) + \mathbf{b}_2)$ as above, and that $f(\mathbf{h}_1)$ may be $G^{-1}_{\mathbf{x}'}(z)$, which is assumed to be uniformly continuous. It follows, allowing $\epsilon = e + e'$:

$$\Pr\Big(\big|\hat{G}^{-1}(\mathbf{x}', z) - G^{-1}_{\mathbf{x}'}(z)\big| > \epsilon\Big) < \delta. \tag{52}$$

as required.

Lemma 5. *For any $\epsilon > 0$ and $\delta > 0$ there exists a mean-field weight distribution $q(\boldsymbol{\theta}_1, \boldsymbol{\theta}_2, \mathbf{b}_1, \mathbf{b}_2)$ such that the probability density functions are bounded:*

$$\Pr\Big(\big|p(y_i = \hat{\mathbf{Y}}_i) - p(y_i = \mathbf{Y}_i|\mathbf{x}', \mathcal{D})\big| > \epsilon\Big) < \delta, \quad \forall \mathbf{x}', y_i, \mathcal{A}. \tag{46}$$

In this lemma, we show that a bound on the inverse c.d.f. used to map Z onto our target implies a bound in the p.d.f. of that constructed random variable to the p.d.f. of our target.

This lemma follows the argument of the simplified construction, with some additional complexity of notation introduced by the requirement that the input random variable was Gaussian rather than Uniform. Here, we complete the proof steps with a univariate y to simplify notation, noting that because we can map $\mathbb{R} \to \mathbb{R}^K$ the multivariate regression follows trivially from the univariate result.

We first note that the result of Lemma 4 can be applied to $z' = \hat{G}(\mathbf{x}', y)$ using an inverted version of our network function such that:

$$\Pr\Big(\Big|\hat{G}^{-1}(\mathbf{x}', \hat{G}(\mathbf{x}', y)) - G^{-1}_{\mathbf{x}'}(\hat{G}(\mathbf{x}', y))\Big| > \epsilon_2\Big) < \delta_2, \quad \forall \mathbf{x}' \in \mathcal{A}, y. \tag{53}$$

We further note that by the triangle inequality:

$$\left|G^{-1}_{\mathbf{x}'}(G_{\mathbf{x}'}(y)) - G^{-1}_{\mathbf{x}'}(\hat{G}(\mathbf{x}', y))\right| \leq \left|G^{-1}_{\mathbf{x}'}(G_{\mathbf{x}'}(y)) - \hat{G}^{-1}(\mathbf{x}', \hat{G}(\mathbf{x}', y))\right| \tag{54}$$

$$+ \left|\hat{G}^{-1}(\mathbf{x}', \hat{G}(\mathbf{x}', y)) - G^{-1}_{\mathbf{x}'}(\hat{G}(\mathbf{x}', y))\right|, \tag{55}$$

and since $G^{-1}_{\mathbf{x}'}(G_{\mathbf{x}'}(y)) = \hat{G}^{-1}(\mathbf{x}', \hat{G}(\mathbf{x}', y)) = \mathbf{x}'$:

$$\leq \left|\hat{G}^{-1}(\mathbf{x}', \hat{G}(\mathbf{x}', y)) - G^{-1}_{\mathbf{x}'}(\hat{G}(\mathbf{x}', y))\right|. \tag{56}$$

Inserting this inequality into the result of Lemma 4, we have that:

$$\Pr\Big(\left|G^{-1}_{\mathbf{x}'}(G_{\mathbf{x}'}(y)) - G^{-1}_{\mathbf{x}'}(\hat{G}(\mathbf{x}', y))\right| > \epsilon_2\Big) < \delta_2, \quad \forall y, \mathbf{x}' \in \mathcal{A}. \tag{57}$$

But we further note that we have assumed that the c.d.f. $G_{\mathbf{x}'}$ is uniformly continous so for any y' and y'', and for any $\epsilon' > 0$ there is an $\epsilon'' > 0$ and vice versa, such that if:

$$|y' - y''| < \epsilon', \tag{58}$$

then:

$$|G_{\mathbf{x}'}(y') - G_{\mathbf{x}'}(y'')| < \epsilon''. \tag{59}$$

It follows that for any ϵ and δ there is a $q(\boldsymbol{\theta})$ such that:

$$\Pr\Big(\left|G_{\mathbf{x}'}(G^{-1}_{\mathbf{x}'}(G_{\mathbf{x}'}(y))) - G_{\mathbf{x}'}(G^{-1}_{\mathbf{x}'}(\hat{G}(\mathbf{x}', y)))\right| > \epsilon\Big) < \delta, \quad \forall \mathbf{x}' \in \mathcal{A}, y \tag{60}$$

and therefore:

$$\Pr\Big(\left|(G_{\mathbf{x}'}(y) - \hat{G}(\mathbf{x}', y)\right| > \epsilon\Big) < \delta, \quad \forall \mathbf{x}' \in \mathcal{A}, y. \tag{61}$$

Next, we remember that $G_{\mathbf{x}'} = \phi \cdot F^{-1}_Z \cdot F_{Y|\mathbf{x}'}$, and that ϕ and F^{-1}_Z are continuous, and therefore:

$$\Pr\Big(\left|(F_{Y|\mathbf{x}'}(y) - F_{\hat{Y}|\mathbf{x}'}(y)\right| > \epsilon\Big) < \delta, \quad \forall \mathbf{x}' \in \mathcal{A}, y, \tag{62}$$

where $F_{\hat{Y}|\mathbf{x}'}(y) = F_Z(\phi^{-1}(\hat{G}(\mathbf{x}', y)))$.

As a final step, we remember that the cumulative density is the integral of the probability density function. Therefore, by Theorem 7.17 of Rudin [1976] and the uniform convergence in the c.d.f.s, it follows that there for any bounds there exists $q(\boldsymbol{\theta})$ such that:

$$\Pr\Big(\left|f_{\hat{Y}|\mathbf{x}'} - f_{Y|\mathbf{x}'}\right| > \epsilon\Big) < \delta, \quad \forall \mathbf{x}' \in \mathcal{A}, y. \tag{63}$$

Writing out the probability density functions fully and mapping the univariate function the multivariate we have:

$$\Pr\Big(\left|p(y_i = \hat{Y}_i) - p(y_i = Y_i|\mathbf{x}', \mathcal{D})\right| > \epsilon\Big) < \delta, \quad \forall \mathbf{x}' \in \mathcal{A}, y_i. \tag{64}$$

□